Synthesis, Structure Determination, and Sol-Gel Processing of Heterometallic Heteroleptic Alkoxide Complexes of Late Transition Metals

Pia Werndrup
Faculty of Natural Resources and Agricultural Sciences
Department of Chemistry
Uppsala

Doctoral thesis
Swedish University of Agricultural Sciences
Uppsala 2005

Acta Universitatis Agriculturae Sueciae
2005:27

ISSN 1652-6880
ISBN 91-576-7026-9

Tryck: SLU Service/Repro, Uppsala 2005

Abstract

Werndrup, Pia. 2005. *Synthesis, Structure Determination, and Sol-Gel Processing of Heterometallic Heteroleptic Alkoxide Complexes of Late Transition Metals*. Doctor's dissertation.

ISSN 1652-6880, ISBN 91-576-7026-9.

The thesis describes synthesis of single-source precursors (SSP) for sol-gel preparation of thin films and nanocomposites. The structures of the SSPs were determined by single-crystal X-ray studies and a new group of heterometallic heteroleptic alkoxide complexes have been described, the $M^{II}_2M^{V}_2(acac)_2(OR)_{12}$ complex, M^{II}= Co, Ni, Zn or Mg, and M^{V}= Ta or Nb, R= Et or Me. Changing to molybdenum oxomethoxide, $MoO(OMe)_4$, instead of tantalum or niobium alkoxide, in the reaction with cobalt acetylacetone provided $Co_2Mo_2O_2(acac)_2(OMe)_{10}$. Nickel acetylacetonate in the reaction with $MoO(OMe)_4$ provided $Ni_2Mo_2O_2(acac)_2(OMe)_{10}$. In order to improve solubility, the acetylacetonate complex was exchanged for $Ni(OR^N)_2$ (R^N= $CHMeCH_2NMe_2$) and the reaction provided $Ni_2Mo_2O_2(OR^N)_2(OMe)_{10}$. The structure of $Ni_2Mo_2O_2(L)_2(OMe)_{10}$, L= acac or OR^N, was determined by EXAFS.

Nanocomposite powder was produced by hydrolysis and condensation of the SSPs, with toluene as solvent. The xerogel powders from $Ni_2Mo_2O_2(OR^N)_2(OMe)_{10}$ were annealed at different temperatures and showed increasing degree of crystallization of the material. At 700 °C, crystallized grains could be seen, with low porosity but a large surface area provided by the grain size (175-250 nm). The oxide powders obtained at 650 °C and 800 °C from $Co_2Ta_2(acac)_2(OMe)_{12}$ showed dense and well-faceted xerogel particles with an even size distribution. Small islands of a crystallized oxide phase could be seen on the surface of the particles.

Thin films were produced by spin-coating on Si and SiO_2. SEM images of the oxide films from $Co_2Ta_2(acac)_2(OEt)_{12}$ revealed smooth and evenly distributed films on the substrates. The different layers were not seen, indicating uniform depositions.

Zeolite Y (12 Å pores) was used for implementation of $M^{II}_2M^{V}_2(acac)_2(OMe)_{12}$. The implemented zeolite complex was studied by EXAFS and the catalysis ability was tested. For modelling experiments, synthesis between $Co_2Nb_2(acac)_2(OMe)_{12}$ and cyclohexylsilsesquioxane was performed and resulted in $Co[(C_6H_{11})_7Si_7O_{12}]_2H_4$. According to the very similar FT of the EXAFS analyses of the implemented zeolite and the Co-silsesquioxane complex, the metallasilsesquioxane complex can serve as a zeolite Y analogue with implemented metal atoms.

Keywords: sol-gel, alkoxide, single-source precursors, nanocomposite materials, zeolite, silsesquioxanes, single-crystal X-ray, EXAFS, SEM.

Author's address: Pia Werndrup, Department of Chemistry, SLU, Box 7015, S-750 07 Uppsala, Sweden. E-mail: Pia.Werndrup@kemi.slu.se

Tillägnas min Pappa

och Ingrid,
som såg annonsen i DN…

"If you want something said, ask a man;
If you want something done, ask a woman"

– Margaret Hilda Thatcher

Contents

Appendix

Papers I-VIII

The thesis is based on the following papers, which will be referred to by their Roman numerals:

I. P. Werndrup, S. Gohil, V. G. Kessler, M. Kritikos and L. G. Hubert-Pfalzgraf, Synthesis, characterization and molecular structures of homo- and heterometallic nickel(II) aminoalkoxides $Ni(\eta^2\text{-}OR^N)_2$ and $Ni(Ni_{0.25}Cu_{0.75})_2(\mu_3\text{-}OH)(\mu\text{-}OAc)(\eta^1\text{-}OAc)_2(\mu,\eta^2\text{-}OR^N)_2(\eta^2\text{-}R^NOH)$ (R^N=$CHMeCH_2NMe_2$). *Polyhedron*, 2001, **20**, 2163-2169.
II. P. Werndrup and V. G. Kessler, Interaction of $Co(acac)_2$ and $Ta(OMe)_5$: Isolation and X-ray Single Crystal Study of the Products. $M^{II}{}_2M^{V}{}_2(acac)_2(OMe)_{12}$, M^{II}=Co, Ni, Zn, Mg and M^{V}=Ta, Nb - A New Class of Heterometallic Heteroleptic Alkoxide Complexes. *J. Chem. Soc., Dalton Trans*., 2001, 574-579. Reproduced by permission of The Royal Society of Chemistry.
III. P. Werndrup, G. A. Seisenbaeva, G. Westin, I. Persson and V. G. Kessler, Single-Source Precursor Approach to Late Transition Metal Molybdate Materials. The Structural Role of Chelating Ligands in the Formation of Heterometallic Heteroleptic Alkoxide Complexes. *Inorg. Chem*. Submitted for publication. Reproduced with permission from Inorganic Chemistry. Unpublished work copyright 2005 American Chemical Society.
IV. P. Werndrup and V. G. Kessler, Application of $M^{II}{}_2M^{V}{}_2(acac)_2(OMe)_{12}$ Derivatives in Sol-Gel Preparation of Oxide and Oxide Nanocomposite Materials for Catalysis. *J. Sol-Gel Sci. Tech*., 2003, **26**, 883-886. Published with kind permission of Springer Science and Business Media.
V. P. Werndrup, M. Verdenelli, F. Chassagneux, S. Parola and V. G. Kessler, Powders and Dense Thin Films of Late Transition Metal Oxide Nanocomposites from Structurally Characterized Single-Source Precursors. *J. Mater. Chem*., 2004, **14**, 344-350. Reproduced by permission of The Royal Society of Chemistry.
VI. P. Werndrup and V. G. Kessler, Bis-silsesquioxane Complex as a Molecular Model of Transition Metal Oxide-Zeolite Nanocomposite. *Inorg. Chem. Comm*., 2004, **7**, 588-591.

Related articles, not included in the thesis

VII. G. A. Seisenbaeva, L. Kloo, P. Werndrup, and V. G. Kessler, Electro-chemical Synthesis, X-ray Single Crystal, IR Spectroscopic, and Quantum Chemical Investigation of Molybdenum and Tungsten Hexamethoxides. *Inorg. Chem.* 2001, **40**, 3815-3818.
VIII. V. G. Kessler, G. A. Seisenbaeva, P. Werndrup, S. Parola and G. I. Spijksma, Molecular Structure Design and Synthetic Approaches to Single-Source Precursors in Sol-Gel Technology. *Mater. Sci.* 2005, Accepted for publication.

Introduction

Today, everyone depends on the materials that are man-made. It is, I think, impossible to live a life without plastics and other new materials. The plastic era started with Bakelite in 1909 and today we have plastics in almost every possible place. If the starting material can be kept simple and inexpensively produced, we will have cheap and easily produced materials. The high-density polyethene plastics (HDPE) *e.g.* is produced from ethene gas and is also environmentally friendly thanks to the carbon dioxide and water produced when it is burned. However, all the materials in demand today are not always so easily produced and not always plastics. There is a need for scratch protection of surfaces, a need for wear resistant surfaces, a need for surfaces with low friction (to lower the amount of excess heat produced), and so on. The list can be made very long.

The new materials can also be catalysts. Catalysts are used in reactions to speed them up and to make them possible at a lower temperature. The Swedish scientist Jöns Jacob Berzelius was the one that coined the term "catalysis" in 1836 [1]:
"*Many bodies have the property of exerting on other bodies an action which is very different from chemical affinity. By means of this action they produce decomposition in bodies, and form new compounds into the composition of which they do not enter. This new power, hitherto unknown, I shall call it catalytic power. I shall also call catalysis the decomposition of bodies by this force*".

Since then, catalysts have been widely used and still are, in *e.g.* plastics syntheses and in car exhaust cleaners. All the enzymes we have in the body are catalysts for biochemical reactions and we would not be around if we did not have all these enzymes in all the necessary reactions for everything we need in our bodies.

Reactions that use catalysts and being of interest today are, *e.g.*, the conversion of methanol into formaldehyde, performed with a $Fe_2(MoO_4)_3$ catalyst; saturation of vegetable fats to make margarine, performed with a Ni-based catalyst; synthesis of pharmaceutical drugs with the desired chirality, performed with zeolite based catalyst (see below); and – probably, the ultimate reaction for catalysis today – the conversion of car exhausts fumes (CO, NO_x, and hydrocarbons) to less polluting gases (CO_2, H_2O, and N_2). In cars today, there is a platinum-based catalyst with a small amount of rhodium. The platinum catalyst converts carbon monoxide and hydrocarbons to carbon dioxide and water. For the conversion of NO_x into N_2, the rhodium catalyst is used. One problem with the car catalysts of today is that they need a rather high working temperature for full conversion, which means that it takes some minutes before the optimal temperature is reached and during that time hardly any of the exhaust is converted. A big step for a better environment would be if the catalyst could work at a lower temperature. Another problem is that the amount of platinum and rhodium are finite, the need for a catalyst based on another metal is rising.

Development of New Materials

Materials for coatings, catalysis, ceramics, *etc*., are produced in several different ways today. A simple, but uncertain, method is the solid-state reaction. In this reaction, oxide or carbonate powders of the precursors are mixed, grinded, put in some form of a mould and calcined in a furnace with a suitable atmosphere. Often, the calcination process takes a long time and the temperature is very high. The grinding process must be repeated sometimes because of defects (uncertainties) of the atomic scale homogeneity, even though the prepared sample may look homogeneous on the macro scale. The reaction takes place at the interface between different grains of the precursors. The newly formed product may hinder further reaction because the grain surfaces of the reactants are no longer in contact and diffusion of the reactants must take place. This may prolong the reaction time. The spinel $MgAl_2O_4$ is prepared this way with a reaction time of one week at 1500 °C [2, 3]. Other materials are prepared at shorter times but most often at quite high temperatures and care must be taken so that the reactants do not evaporate or melt at these high temperatures. It is important to check that the product has the correct stoichiometry because decomposition of the precursors does not always follow the prediction. The better homogeneity of the sample on the nanometre scale level the better control of the surface activities and the reactions taking place.

A possible way to tackle the problem with low homogeneity due to mixing-problems or difficulties to control stoichiometry of two or more reactants is to use molecular single-source precursors (SSPs). These precursors decompose on heating into the desired product. This product can be a nanocomposite *i.e.* a solid structure with nanometre scale repetitions of the phases that constitutes the structure. The precursors may require several steps in preparation and they still need high temperatures to decompose. Preparing thin films on various substrates can be performed by several methods. Electrochemical methods have been used for a long time and involve cathodic deposition – electroplating with two metal electrodes in an electrolyte and an external field across the electrodes, the metal ions in the electrolyte are deposited on the cathode, or anodic oxidation – the same set-up but the metal is the anode and the film is produced on it. The electrolyte is a salt or acid solution. Physical methods – sputtering, pulsed laser deposition (PLD) and molecular beam epitaxy (MBE) – produce high-quality materials but the methods use expensive and complex equipment at high vacuum. Sputtering uses a high voltage over an anode (the substrate) and a cathode, consisting of the material used for coating the substrate. In the high vacuum, a residue of an inert gas, *e.g.* argon, is excited from the potential drop. Cations are produced and accelerate towards the cathode where material is released. The material condenses on the substrate and a thin film is produced. The pulsed laser deposition method uses ablation of material from a target, obtained with a high-energy laser beam. The material forms a plasma, which deposits on the substrate. Stoichiometric material is formed on the substrate and the method works at relatively low vacuum, not so common among the different physical deposition methods available [4]. If crystalline layers on the substrate are important then the molecular beam epitaxy method can be used. The substrate is heated in a chamber with very low pressure.

The material sources are positioned opposite the substrate. The sources are heated and material is emitted as a beam. This molecular beam hits the substrate and the material can rearrange into a crystalline layer. The MBE method has mostly been used for Group 13 and 15 (Al, Ga, In, and N, P, As, Sb) and Group 12 and 16 (Zn, Cd, Hg, and S, Se, Te) to produce semiconductors [5]. The physical methods are often successful for small surfaces, if the equipment exists; otherwise they are very expensive methods. It can be difficult to deposit on large surfaces or a complex shape of the substrate surface. Trying out new materials on different substrates in small series can become very expensive with these methods due to high initial costs.

If atomic scale homogeneity of the product is important the answer to the problem might be Chimie Douce or *Soft Chemistry Methods*. Chemical vapour deposition (CVD) is one of the methods and produces high purity thin films. The precursors are heated until they are gasified and the reactants decompose on the substrate. Use of single-source precursors will make the thin films even higher in quality. Thin films of the spinel $MgAl_2O_4$ is prepared with CVD by decomposing *e.g.* $[MgAl_2(OBu^t)_8]$ [6] or $Mg[Al(OPr^i)_4]_2$ [7]. The problems with CVD are that the precursors may decompose with the wrong product formed or that the precursors may decompose at different temperatures, thus making the reaction impossible. Impurities of carbon and hydrogen are also a common problem. Soft chemistry methods also involve sol-gel preparation of a homogeneous solution with the reactants in a suitable solvent. With the solvent evaporating, a homogeneous gel is formed due to simultaneous hydrolysis and condensation. The gel is heated in a furnace and the organic residues are burnt off. Crystallization takes place, often at a much lower temperature than with solid-state reactions. The spinel $MgAl_2O_4$ may be prepared by soft chemistry method with the reaction of $Mg(OCH_3)_2$ and $Al(O(CH_2)_3CH_3)_3$ at 250 °C [3, 8].

Thin films are also produced by sol-gel methods. A solution of the precursor is prepared with an easily evaporating solvent and the substrate is dipped into the solution or the solution is poured onto the substrate while spinning. As the solvent evaporates a coating on the substrate is formed. The substrate is heated in a furnace and a thin oxide layer of required composition is formed. A great advantage with the sol-gel method is the possibility to use very large substrates because no machine needs to be used when the coating is performed, the size of the furnace can be the limiting factor. With physical methods and CVD, problems with a very thin beam of material condensing on the substrate can cause unevenly coated samples, especially if the substrate must be moved to be able to coat a larger part of the surface.

Nanocomposite powders can be of four different types: intra-type, inter-type, intra/inter-type and nano/nano-type. The intra-type has large (micro-sized) particles imbedded with another kind of nano-sized particles. This makes it stronger and tougher than single-phase materials. The nano-sized particles are surrounding the larger particles in the inter-type and the intra/inter-type has both kinds of nano-sized particles. The most interesting nanocomposite type is the nano/nano-type because here both particles are nano-sized and this provides new

features such as very large surface area, superplasticity, and microporosity. Nanocrystalline powder (the nano/nano-type) of the $MgAl_2O_4$ spinel [9, 10] or the $ZnFe_2O_4$ magnetic spinel [11] can be produced by different methods, among them sol-gel preparation. However, the sol-gel method is often too expensive for an industrial production and most often the more traditional methods already described must be used.

Alkoxides

In the search for new materials for applications in modern technology, metal alkoxides and their derivatives are of great interest. An oxide material is fairly easy to obtain from the alkoxides, and nanocomposites such as catalyst materials can be produced with a high degree of control and purity. Alkoxides ($M(OR)_n$) are compounds with one or more metal atoms or semi-metal atoms (M) with alkoxy groups (OR) as ligands. Alkoxy ligands are produced by stripping the hydrogen atom from an alcohol molecule or by dividing an ether molecule so that the oxygen is given to the alkoxy group. Alkoxides are analogues of hydroxides and are known for almost all the elements in the periodic table.

Synthetic Routes to Homometallic Alkoxides

Alkoxides can be prepared by several different synthetic routes [12-15]. One of the seven synthetic methods below can often be used to produce any desired metal alkoxide.

- *Method 1* - Direct reaction between metal and alcohol.

$$M + n\ R\text{-}OH \rightarrow M(OR)_n + n/2\ H_2\ (g)$$

This method is only used for the most reactive metals such as alkaline metals, alkaline earth metals, rare earth metals, and aluminium. For a typical reaction, a large surplus of the alcohol is needed. For Mg, Ca, Al and the lanthanides a catalyst (*e.g.* a small amount of iodine) is needed for the reaction to occur.

- *Method 2* - Anodic oxidation of metal in alcohol.

This method works for less reactive metals such as Zr, Ta, Nb, Co, Fe and Ni. An electroconductive additive (a halide) must often be added. In the case of Co, Fe, and, Ni, the halide radical released attacks the electrode surface and a solvated metal halide is produced. The metal halide is then reduced to a metal alkoxide at the cathode. The lithium chloride can react with the solvent alcohol and produces a lithium alkoxide complex along with hydrogen and a chlorine radical. This radical reacts further with the alcohol and produces hydrogen chloride and an aldehyde [16].

$$LiCl + R\text{-}CH_2\text{-}OH \rightarrow Li\text{-}O\text{-}CH_2\text{-}R + \tfrac{1}{2}\ H_2\ (g) + Cl^{\cdot}$$

$$2\ Cl^{\cdot} + R\text{-}CH_2\text{-}OH \rightarrow 2\ HCl + R\text{-}CHO$$

The metal alkoxide produced by anodic oxidation is often insoluble in the solvent and therefore precipitates. A drawback can be the formation of *e.g.* a lithium-

nickel heterometallic alkoxide complex, instead of the expected nickel alkoxide complex [17]. With Zr, Nb and Ta, the metal alkoxide complex is formed directly at the anode without formation of a metal halide solvate.

- *Method 3* - Metal oxide or hydroxide reaction with alcohol.

  $M'\text{-}O + 2\ R\text{-}OH \rightleftharpoons M'\text{-}(OR)_2 + H_2O$

  $M''\text{-}OH + R\text{-}OH \rightleftharpoons M''\text{-}OR + H_2O$

Both these reaction routes were claimed to produce alkaline metal and alkaline earth metal (Sr or Ba) alkoxides. Since the reactions above are equilibrium reactions they cannot be used for drying alcohols. Alkoxides of Mg, Ca or Al are often used for obtaining water-free alcohol since their reactions with water are irreversible.

- *Method 4* - Reaction between MX_n (X = H, alkyl, C≡C, ≡N, NH_2, NR_2, SH, $N(SiR_3)_2$, …) and alcohol.

  $MX_n + n\ R\text{-}OH \rightarrow M(OR)_n + n\ HX$

Here, the hydrogen in the alcohol interacts with the produced anion (from *e.g.* the metal hydride) and HX is produced along with the metal alkoxide. Alkaline hydrides are often used as start materials. Metal amides of Cr(II), Mn(II), Zn(II), Cd(II) and Pb(II) are used in alcoholysis and produce metal alkoxides, but the amides themselves must often be synthesized first as they are rarely commercially available.

- *Method 5* - Metathesis between two different metal complexes.

  $MX_n + n\ M'OR \rightarrow M(OR)_n + n\ M'X$ X=halide

This is the most common method for synthesis of metal alkoxides. The solvent is usually an alcohol mixed with another organic solvent used to decrease the solubility of M'X. If M'OR is NaOR then NaCl is produced, which is almost always insoluble in the organic solvent. Very often an ammonia solution is used, providing NH_4Cl, also insoluble in organic solvents. Furthermore, if the metal alkoxide is soluble in the solvent, purification of the alkoxide is simplified thanks to the precipitation of NaCl. One disadvantage of this method is the formation of bimetallic complexes. However, this can be avoided if ammonia is used instead of alkaline alkoxides. The purification of the metal alkoxides is in practice more difficult than in theory; it is often impossible to precipitate M'X in such a manner that it can be removed without great effort.

- *Method 6* - Alcohol exchange or transesterfication.

  $M(OR)_n + n\ R'\text{-}OH \rightarrow M(OR')_n + n\ R\text{-}OH$

  $M(OR)_n + n\ R''COOR' \rightarrow M(OR')_n + n\ R''COOR$

The alcohol produced in this reaction can normally be distilled off, or the new metal alkoxide can be precipitated to enhance the yield. Alkoxy groups formed from alcohols with high boiling point can be exchanged with alkoxy groups from alcohols with low boiling point. A drawback is that it can be difficult to exchange all of the alkoxy groups in the complex leaving a mixed ligand complex. Ramified

alkoxy groups are especially difficult to exchange due to stability of the partially exchanged complex.

- *Method 7* - Redox reaction of a metal alkoxide.

This method is mainly used in reactions with oxygen, peroxides or halogens and with Mo, U, W or Eu alkoxides. $[Eu_4(OPr^i)_{10}(HOPr^i)_3]\cdot 2\ HOPr^i$ is oxidized to $Eu_5O(OPr^i)_{13}$ on the addition of oxygen to a solution of the first complex [18]. It is not, however, a very common synthesis method.

Synthetic Routes to Heterometallic Alkoxides

The seven methods described above are the present ways to produce homometallic alkoxides. Producing heterometallic alkoxides, *i.e*. alkoxides containing two different metal atoms, requires different approaches. There are two major routes to obtain heterometallic alkoxide complexes.

Reaction between two alkoxide complexes.

$$M(OR)_n + q\ M'(OR)_m \rightarrow MM'_q(OR)_{n+qm}$$

This route is effective if one of the complexes is an alkaline metal or alkaline earth metal alkoxide and the other is an alkoxide of a transition metal, preferably multivalent [19].

Reaction between a metal halide and an alkaline metal alkoxide.

$$MX_n + n\ M'M''(OR)_m \rightarrow MM''_n(OR)_{mn} + n\ M'X\ (s)$$

This route is used when one metal alkoxide is difficult to access, whereas the halide complex can be easily produced [20]. The reaction is simplified with the precipitation of the new metal halide, making the purification process easier.

Although, intriguing and difficult to access, the goal is not only to obtain heterometallic alkoxides for fundamental studies. They should, preferably, be suitable for sol-gel processing and implementation in different matrices such as zeolites (discussed below). The ligands play a big role in the complexes, and changing the ligands greatly differ their chemical behaviour and how they act in sol-gel preparations. Comparison of two complexes of $Ti(OR)_4$, with R= Et and Pr^i, shows that the ethoxide complex gives spherical monodispersed TiO_2 particles when hydrolyzed; the hydrolysis is slower than the condensation which gives larger particles [21]. The isopropoxide complex, with somewhat bulkier ligands, produces polydispersed particles of TiO_2 with irregular shapes when hydrolyzed. The hydrolysis and condensation take place simultaneously producing small, irregular particles. This difference in particle size can be credited to the bulkier ligands of the isopropoxide complex, because monodispersed oxide powders are mainly produced from alkoxides with small alkoxide groups.

Synthetic Routes to Heteroleptic Alkoxides

Heteroleptic alkoxide complexes, *i.e*. alkoxide complexes with two or more different ligands, can be prepared by chemical modification – a metal alkoxide reacts with an acidic organic ligand, see equation, or by reaction of the metal alkoxide with a β-diketonate (*e.g.* acetylacetone (Hacac, H_3C-C(O)-CH_2-C(OH)-CH_3)) or a carboxylate metal complex (with the same or different metal atom).

$$M(OR)_n + m\ HZ \rightarrow M(OR)_{n-m}Z_m + m\ ROH \qquad Z=\text{acidic organic ligand}$$

Complexes with a β-diketonate or a carboxylate ligand are less reactive to hydrolysis than an ordinary alkoxide complex due to larger negative charge on the carboxylate or β-diketonate ligand and a chelating effect. When a $Ti(OR)_4$ complex reacts with Hacac, a heteroleptic complex, $Ti(OR)_3$(acac), is formed along with the alcohol ROH (R= Pr^i or Bu^n for example). When $Ti(OR)_3$(acac), is hydrolyzed the acac ligand is not removed due to the chelating effect of the ligand and a stable sol is formed instead of precipitation of TiO_2 particles.

The reaction with a β-diketonate complex is another way to prepare heterometallic alkoxide complexes but may also result in heterometallic heteroleptic alkoxides. When heterometallic complexes were accessed, the solvent was purely hydrocarbon based, such as toluene or hexane [22-24]. If alcohol was added, it acted as a Lewis base and formation of heterometallic complexes was interrupted and ligand exchange occurred instead [25]. The use of different ligands in the precursor complexes is a way to control the gel powder porosity and the gel film density when producing materials. With all-alkoxide precursors the gel powders have low porosity due to easy hydrolysis and condensation reactions with small amounts of organic residues that are difficult to release by heat-treatment. With β-diketonate ligands in the precursor, or other ligands that are more resistant to hydrolysis, the gel powders are more porous due to the fact that the ligands are spacious and need higher temperature before they decompose and the rest of the powder are then already set in shape.

The gel films produced by spin-coating with all-alkoxide precursors are often porous with a strong gel network and with low density [26]. The hydrolysis and condensation is too fast in the material to be able to make a fully dense film. Dense gel films with low porosity can be made fairly easily with β-diketonate containing precursors probably due to the β-diketonate ligands, that, in spite of their volume, arrange themselves in positions with the ligands on the particle surfaces. Hacac is produced from rearrangements in the network and evaporates from the gel films at lower temperature than the acac ligand itself is thermally or oxidatively decomposed. This densifies the gel in a way not possible for gel films without the β-diketonate ligand [27]. In chemical vapour deposition, the rate of ligand elimination plays a major role in the film thickness and particle size. The faster the ligands can be eliminated the better the crystalline film can grow [6]. If the ligands are bulky, as *e.g*. the *tert*-butoxy ligand compared to the isopropoxide ligand, the vapour pressure can be increased due to reduced nuclearity and the elimination of the ligands is increased.

Classification by Structure of Alkoxide Complexes

Metal alkoxide complexes can have very intricate structures due to formation of oligomeric and sometimes even polymeric aggregates. Formation of alkoxy bridges, M-O(R)-M', help the complexes to obtain maximal (and preferred) coordination even though the number of bonded ligands per metal atom are too few. The number of metal atoms in the complex categorizes the complexes. Optimal coordination is obtained by chelating ligands (in writing: η^x with x=1-4, depending on how many atoms in the ligand that are involved in the formation), Figure 1 a, or by a shared (bridging) ligand atom (in writing: μ_x where x=2-6, depending on how many metal atoms the shared atom is connected to and μ_2 is often just denoted μ), Figure 1 b.

Mononuclear complexes – highly charged metal ions where the number of OR-ligands satisfies the coordination requirements, the ligands are often large and ramified with chelating abilities, Figure 1 a.

Binuclear complexes - the two metal atoms are connected *via* an oxygen atom in the ligand (the oxygen in an OR group). Usually at least two alkoxy bridges are connecting the metal atoms and thus stabilizing the complex, Figure 1 b. Mo and W complexes can have metal-metal bonds to stabilize the complex (without any bridging ligand), the multiplicity depends on the number of ligands and nature of them, Figure 1 c.

Trinuclear complexes - are often triangular structures, Figure 1 d, linear chains, Figure 1 e, or non-linear chains with the same type of connections as in the binuclear complexes.

Tetranuclear complexes - have several different types of configuration, some are very uncommon. The tetrahedral configuration has a core of μ_4-O and four metal atoms connected by the oxoligand, but this is not a common configuration, Figure 2 a. The $Ti_4(OR)_{16}$-type is very common and is built up by a M_4-rhomb with 2 μ_3-O and 4 μ-O, Figure 2 b. The R-groups are most often primary alkyl groups for the 3d-metals.

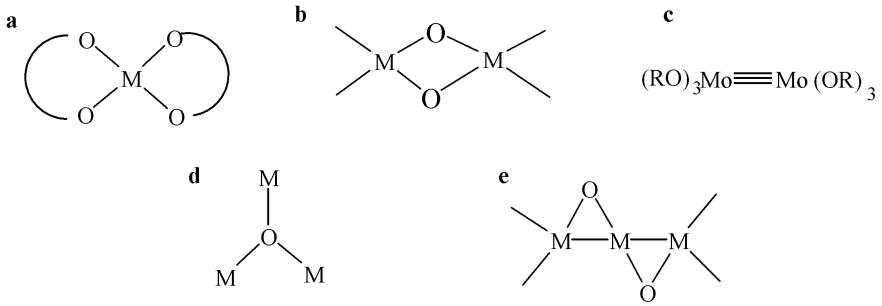

Figure 1. Schematic representations of a mononuclear complex (a), binuclear complexes (b and c) and trinuclear complexes (d and e).

The cubane-like configuration contains metal atoms in four opposite corners of a cube and oxygen atoms in the other corners (4 μ_3-O), Figure 2 c. One configuration, called butterfly, depends, most often, on metal-metal bonds and therefore only low-valent Mo, W and Re display this one. It is built up by 2 M_3-triangles, Figure 2 d. The butterfly configuration is possible even in the absence of metal-metal bonding but then the "wings" are bonded to each other *via* a hydrogen bond. Examples without a metal-metal bond are the $Al_4(\mu_4\text{-O})(\mu\text{-OPr}^i)_5$ complex [28] and the $[Eu_4(OPr^i)_{10}(HOPr^i)_3]\cdot 2\ HOPr^i$ complex [18]. The $Al_4(OPr^i)_{12}$-type (the propeller type) has an octahedron (with Al in the centre) in the centre and three tetrahedra of Al connected *via* pairs of OR-bridges, Figure 2 e. A heterometallic example is the $Nd[Al(^iPrO)_4]_3$ with the Nd atom in the centre of the complex [29].

Pentanuclear complexes - belong most often to either of two different coordinations, the trigonal bipyramid, Figure 3 a, and the square pyramid, Figure 3 b, both with a μ_5-O in the centre of the M_5O-cluster, or a structure with two triangles sharing a vertex. Many lanthanide oxo-isopropoxide complexes belong to the square pyramidal coordination, *e.g.* the $[Eu^{III}_4Eu^{II}O(OPr^i)_{12}(HOPr^i)]\cdot\ HOPr^i$ complex [30] and $Ln_5O(OPr^i)_{13}$, Ln = Nd, Gd or Er [31].

Hexanuclear complexes - the most common ones are an octahedral M_6-arrangement with a μ_6-O in the centre, Figure 3 c, or a structure with two M_3-triangles connected by the ligands, the double propeller type, Figure 3 d.

Complexes with 7, 8 or 9 metal atoms are not so common and not discussed here.

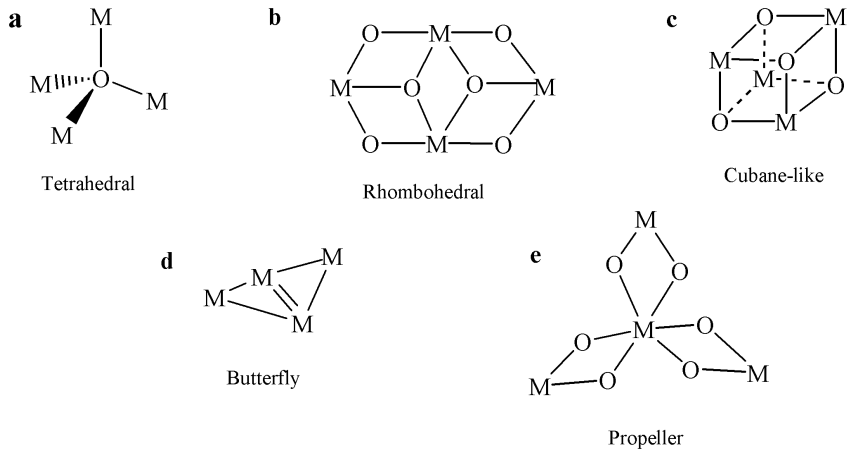

Figure 2. Schematic representation of tetranuclear complexes (a, b, c, d and e).

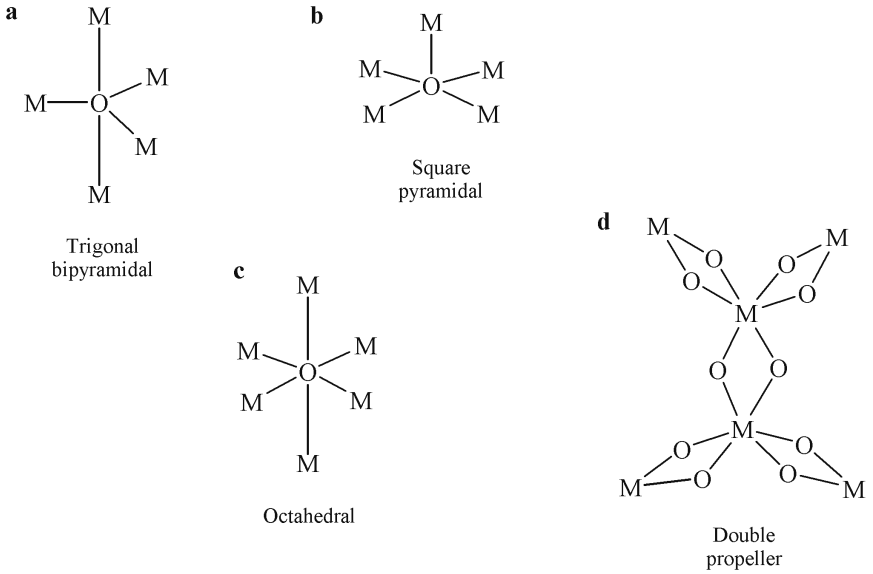

Figure 3. Schematic representation of pentanuclear complexes (a and b) and of hexanuclear complexes (c and d).

The possible structure types of different alkoxide complexes and their relation to materials preparation can be summarized by the Molecular Structure Design Concept – a concept based on three steps for determining the structure type required for the complex to be useful in the preparation of the material wanted [12-15]. First step is to choose structure type, from the ones described above. Second step is to calculate the number of donor atoms necessary for the chosen structure type. Third step is to choose the proper ligands, with enough donor atoms to fulfil the coordination requirements for the structure. A careful choice of ligands will make the structure complete. Choosing ligands with bridging capabilities will make the structure more protected, so that the metal core will be stable until the material is formed.

Sol-Gel Preparation

The sol-part of sol-gel means a liquid suspension of particles of 1 nm to 1 μm in size and the gel-part means a solid with a three-dimensional network encapsulating the solvent it was produced in. Four important steps are involved in the making of oxide materials – sol making or hydrolysis of the precursor material, aging of the gel, solvent removal, and heat treatment of the product, Scheme 1 [14, 32, 33]. Often, in order to get a sol, hydrolysis of metal alkoxides is performed, because using inorganic metal salts as starting material for sol making will produce anions, and micelle formation is common. This will strongly influence the morphology of the particles produced from this sol and may decrease their stability.

Two different reactions occur when water is added, hydrolysis and condensation.

$M\text{-}OR + H_2O \rightarrow M\text{-}OH + R\text{-}OH$ *Hydrolysis*
$M\text{-}OH + XO\text{-}M \rightarrow M\text{-}O\text{-}M + XOH$ *Condensation*, X=H or R

The amount of water added will influence the rate of hydrolysis and condensation; the more water added, the more network is formed. If not enough water is added no gel can be formed due to too few M-OH groups for the condensation step. A gel with a large network is formed when the hydrolysis step is the rate determining one.

Adding the water slowly, increasing the pH, changing the solvent, or changing the temperature can control this. Aging is the transformation the gel undergoes after all the water has been added; more cross-links are formed and some solvent is excluded. When evaporation of the solvent starts, the gel changes and the pores decrease in size due to high capillary pressure. A gel dried by ordinary evaporation of the solvent is called xerogel.

Sometimes the gel tends to crack because of the high capillary pressure. One way to avoid this is to use a supercritical drying method yielding a crack-free aerogel. Heat treatment of the gel is performed to make the gel absolutely free of solvent and free of the ligands, leading to a product that is denser and/or crystalline. At much lower temperatures, than with solid-state methods, oxide materials are produced and can be used as catalysts.

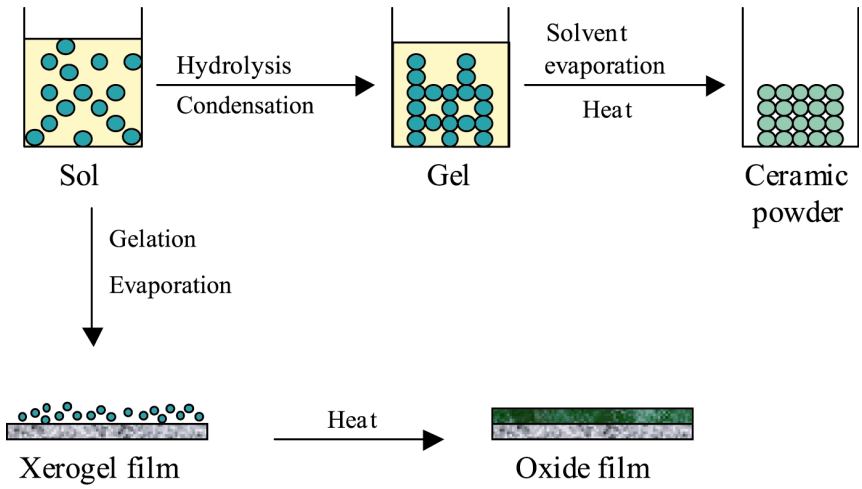

Scheme 1. The different steps in the sol-gel process.

Zeolites

Zeolites are a group of aluminosilicates that are characterized by a network, leaving tunnels where cations or neutral molecules can be trapped. The zeolites can be used as molecular sieves, desiccants, ion exchangers, and water softeners. A new use for zeolites is as matrices for catalysts, where a metal complex is trapped inside the tunnel. Gaseous compounds are then pushed through the zeolites and a chemical reaction occurs. The constraining environment in the zeolite matrix stabilizes the trapped metal complex. A stable metal complex will raise the catalytical activity and using zeolites as support for metal catalyst makes the separation from the solvent easy in contrast to non-trapped metal catalyst. The use of zeolites for chiral selectivity of molecules or chiral catalysis is of importance for the pharmaceutical industry because of need to separate enantiomers. There are several reports of chiral metal complexes being trapped inside the zeolite tunnels, allowing a selective reaction to take place [34-36]. The zeolites are often commercially made by crystallizing gels at 60-100 °C. Zeolite A is rhombohedral [37] and built by cube-octahedra which consists of both smaller and larger cavities, but with a small "entrance", approx. 2 Å. Zeolite Y has a cubic symmetry and larger cavities, approx. 12 Å, Figure 4.

Oxidation of alkanes to alcohols and ketones can be performed by an iron-phtalocyanine complex trapped in a zeolite Y matrix with different oxygen donors, iodosobenzene ($C_6H_5.IO$) or *tert*-butylhydroperoxide, and some interesting features are seen [38]. The encapsulated iron complex has much higher catalytical activity than the same complex in solvated form. The iron complex stays active for a longer period of time than the solvated one and the selectivity changes for the encapsulated complex so that a less bulky cycloalkane is oxidized faster than a bulkier one with iodosobenzene as the oxygen donor, *i.e.* greater reactant shape selectivity with the zeolite complex.

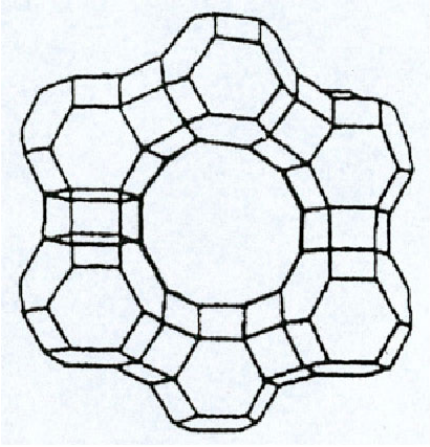

Figure 4. A schematic representation of Zeolite Y, showing the tunnel system from a top section. From Sabater *et. al*. [35].

Oxidation of *n*-octane by the iron-phtalocyanine complex can be performed with greater regioselectivity at the end of the chain if the iron complex is encapsulated into zeolite Y.

General Methods

Synthesis

All manipulations were carried out in a dry nitrogen atmosphere using Schlenk technique or a glove box.

Synthesis of Single-Source Precursors

$[Ni(\eta^2\text{-}OR^N)_2]$ $Ni(\eta^2\text{-}OR^N)_2{\cdot}C_7H_8$ (R^N=$CHMeCH_2NMe_2$) was prepared by addition of Na(s) to HOR^N with subsequent addition of $Ni(NH_3)Cl_2$ [17]. Solvent free $Ni(\eta^2\text{-}OR^N)_2$ was obtained by sublimation of $Ni(\eta^2\text{-}OR^N)_2{\cdot}C_7H_8$ at 93-95 °C and 10^{-2} mm Hg.

$[CuNi_2(OCOC_2H_5)_3(OR^N)_3(R^NOH)]$ Solid $Cu(OCOC_2H_5)_2$ was dissolved in a toluene solution of $Ni(OR^N)_2$ giving a turquoise solution. The latter was evaporated and the residue redissolved in tetrahydrofuran and methanol and left overnight at -30 °C. A light blue crystalline solid was collected by filtration.

$[Ni(Ni_{0.25}Cu_{0.75})_2(\mu_3\text{-}OH)(\mu_2\text{-}OAc)(OAc)_2(\mu_2,\eta^2\text{-}OR^N)_2(\eta^2\text{-}R^NOH)]$ Solid $Cu(OAc)_2{\cdot}(H_2O)$ was added to a solution of $Ni(OR^N)_2$ in a toluene-methanol (5:1) mixture giving a dark blue turbide solution. It became transparent in an hour, after the precipitation of grey-blue sediment that contained only nickel. The filtrate was evaporated to dryness and the green-blue residue was redissolved on heating in tetrahydrofuran and hexane. Turquoise crystals were obtained at 0 °C overnight.

$[M^{II}_2M^V_2(acac)_2(OMe)_{12}]$ Water-free $M^{II}(acac)_2$ (M^{II}=Co, Ni, Zn or Mg and acac=$H_3CC(O)CHC(O)CH_3$) and $M^V(OMe)_5$ (M^V= Ta or Nb) were dissolved in dry toluene. The solution was heated to 60 °C and then slowly cooled to 4 °C. Crystals of $M^{II}_2M^V_2(acac)_2(OMe)_{12}$ precipitated practically in a quantitative yield. The solvent was removed by decantation and the crystals were dried *in vacuum* at room temperature.

$[Co_2Mo_2O_2(acac)_2(OMe)_{10}]$ $MoO(OMe)_4$ was dissolved in dry toluene. $Co(acac)_2$ was dissolved in the molybdenum solution and the solution was refluxed. The solution was decantated and cooled. Purple crystals of $Co_2Mo_2O_2(acac)_2(OMe)_{10}$ precipitated at 4° C.

$[Ni_2Mo_2O_2(L)_2(OMe)_{10}]$, L=$OR^N$ or acac. $MoO(OMe)_4$ was dissolved in dry hexane. $Ni(OR^N)_2$ or $Ni(acac)_2$ was dissolved in the molybdenum solution and the solution was refluxed. After cooling, dry toluene was added and the solution was refluxed again. The solution was decantated and small greenish crystals of

$Ni_2Mo_2O_2(L)_2(OMe)_{10}$ precipitated at 4° C. The decantated solution was stored at -30° C. $MoO(acac)(OMe)_3$ and $[MoO_2(L)(OMe)]_2$ precipitated after several weeks.

$[M^{II}_2M^{V}_2(acac)_2(OEt)_{12}]$ Water-free $M^{II}(acac)_2$ (M^{II}= Co or Ni) and $M^{V}(OEt)_5$ (M^{V}= Ta) were dissolved in dry toluene. The solution was heated to 60 °C and then slowly cooled to 4 °C. Crystals of $M^{II}_2M^{V}_2(acac)_2(OEt)_{12}$ precipitated practically in a quantitative yield. The solvent was removed by decantation and the crystals were dried *in vacuum* at room temperature.

Preparation of Oxide Materials

Hydrolysis. $Ni_2Mo_2O_2(OR^N)_2(OMe)_{10}$ or $M^{II}_2M^{V}_2(acac)_2(OMe)_{12}$ (M^{II}= Co or Ni and M^{V}= Ta or Nb) was dissolved in toluene to make an approx. 5% solution. Distilled water was shaken vigorously with diethyl ether, making the water 1.2% of the diethyl ether. Equimolar amount, regarding the number of alkoxy groups, of the water solution in diethyl ether was added slowly with a syringe to the complex solution on stirring during 1.5 h, converting it to a viscous sol. It was then poured into a dish and the solvent evaporated leaving a fine powder.

Nanophase powder preparation. To produce nanophase powder of $Ni_2Mo_2O_2(OR^N)_2(OMe)_{10}$, $Co_2Ta_2(acac)_2(OMe)_{12}$, $Ni_2Ta_2(acac)_2(OMe)_{12}$ or $Co_2Ta_2(acac)_2(OEt)_{12}$, the samples were hydrolyzed with subsequent evaporation of the solvent. Heating in air was performed in a Carbolite CWF 1300 furnace at 5 °C·min^{-1} or a Comecta SA 3L Furnace at 10 °C·min^{-1} to different annealing temperatures. The agglomerate size and crystallinity of the powders were studied with a Topcon EM-002 B Ultrahigh resolution analytical electron microscope (TEM). SEM was performed on the powders with a Hitachi S800 scanning electron microscope or with a LEO 1550 high-resolution scanning electron microscope. Thermogravimetric analysis was obtained with the Mettler Toledo Star^e System.

Film preparation. Gel films were deposited on Si and SiO_2, using a Suss Microtec RC8 Gyrset spin coater, by adding 0.1 ml of a 0.14-0.28 M filtrated toluene solution of $Co_2Ta_2(acac)_2(OMe)_{12}$ or $Co_2Ta_2(acac)_2(OEt)_{12}$. Thicker films were produced by adding multiple layers with intermittent heating at 150 °C for 5 min. The films were annealed in air in a Carbolite CWF 1300 furnace at varying temperature and time. The morphology of the films was investigated with a Hitachi S800 15 kV scanning electron microscope (SEM). The roughness of the film surface was investigated with a Picoscan-5 Molecular Imaging atomic force microscopy (AFM).

Zeolite Implementation

Zeolite interaction. 12 Å NaY zeolite (Haldor Topsoe) was heated at 400 °C for 1 h for dehydration. $Co_2M^{V}_2(acac)_2(OMe)_{12}$ (M^{V}= Ta or Nb) was dissolved in dry toluene making the solution purple. The zeolite was then added and an exothermic reaction took place, the solid phase turned clear blue almost immediately and the solution became colourless. The solvent was evaporated and the dry solid was found to be its original white. The zeolite product was heat-treated at 400 °C for

1 h, producing an oxide from the original metal complex. The catalytical activity was tested by the reaction of complete oxidation of methanol in gas phase and was performed in a flow-type reactor. The products were analyzed by Mod-3700 gas chromatograph equipped with a 3 m Carbowax 20 M column at 100 °C using a FI detector. Analysis for gas products was carried out on a Chrom-5 apparatus with a 1 m CaA molecular sieve column at 30 °C using a TC detector.

$[Co[(C_6H_{11})_7Si_7O_{12}]_2H_4]$ $Co_2Nb_2(acac)_2(OMe)_{12}$ was dissolved in toluene and $(C_6H_{11})_7Si_7O_9(OH)_3$ was added. The solution was refluxed for 30 minutes and thereafter cooled to 4 °C for 48 h. Pink flakes of $Co[(C_6H_{11})_7Si_7O_{12}]_2H_4$ precipitated.

Characterization

The metal ratio in the bimetallic complexes was determined on a JEOL-820 scanning electron microscope (SEM), supplied with a Link AN-10000 energy dispersive spectrometer (EDS), with air hydrolysis. IR spectra of nujol mulls were registered with a Perkin Elmer FT-IR spectrometer 1720 X or a Nicolet Magna-IR 560 spectrometer. UV spectra were recorded using a Hitachi U-2001 spectrophotometer. Mass spectra (electron beam ionisation, direct probe introduction) were recorded using JEOL JMS-SX/SX-102A mass-spectrometer (performed by Mr. Suresh Gohil). ^1H NMR spectra were obtained for solutions in anhydrous $CDCl_3$ with a Bruker 400 MHz or 600 MHz spectrometer (performed by Mr. Rolf Andersson). Thermal behaviour was analyzed by thermogravimetry (TG) analysis using a Perkin Elmer Thermogravimetric Analyzer TGA7 equipped with P E Thermal Analysis Controller TAC 7/DX or a Setaram Setsystem 16/18 coupled TGA/DSC equipment. X-ray powder diffraction (XRD) of the obtained phases was recorded with a Philips PW 3710 diffractometer with $CuK\alpha_1$ radiation (λ=1.54056 Å) or with a Phillips SR5056 temperature programmed diffractometer.

X-ray crystallography

All the compounds studied are sensitive to ambient atmosphere and were therefore placed into Lindeman glass capillaries, sealed under vacuum, for data collection. The data were collected using SMART CCD 1K diffractometer at 22°C. All calculations were performed using the SHELXTL program package [39] Version 5.3. The structures were solved by standard direct methods; the coordinates of the metal atoms were taken from the initial solutions and the other non-hydrogen atoms were located in subsequent Fourier syntheses. The structures were refined by full matrix least-squares in an isotropic and anisotropic approximation. The positions of the hydrogen atoms were calculated geometrically and included in the final cycles of the refinement in isotropic approximation. Absorption correction, using SADABS, was performed, where needed.

EXAFS Analysis

A core electron of an atom can be excited if electromagnetic radiation of the suitable energy hit the atom. The radiation must have high intensity and a synchrotron is most often used to obtain these high intensities at required energies; they fall into the X-ray region. The core electron creates a photoelectron, which can interact with surrounding atoms and backscattering waves are formed. An experimental set-up in transmission or fluorescence mode, depending on the sample concentration, determines the total absorption as a function of energy.

Three distinct regions of the X-ray absorption spectrum can be detected. The first region is the pre-edge, which ends just before the excitation energy level of the atom. The edge, the second region, is called XANES (X-ray Absorption Near Edge Structure) and includes the excitation energy level and up to 50 eV above the edge. The third region, called EXAFS (Extended X-ray Absorption Fine Structure), starts after the XANES region and continues up to 1000 eV after the edge. The oscillations in this region are examined and the raw data is background corrected, normalized, and energy converted (*k*-space), usually k^3-weighted, Figure 5 a. Finally a Fourier transformation into distance space (r-space) is performed. The Fourier transformation produces a graph that can be used for examination of the different scattering contributions in the sample, Figure 5 b [40].

The EXAFS data in Papers **III**, **IV** and **VI** were collected in transmission and fluorescence mode, at the wiggler beam line 4-1 at the Stanford Synchrotron Radiation Laboratory (SSRL), Stanford, USA. SSRL operated at 3.0 GeV and at a maximum current of 100 mA. The EXAFSPAK program package was used for all data treatment and refinement [41]. The EXAFS oscillations were obtained after performing standard procedures for pre-edge subtraction, normalization and spline removal. The k^3-weighted model functions were calculated using *ab initio* calculated phase and amplitude parameters obtained by the FEFF6 or FEFF7 program packages (versions 6.01 or 7.01, respectively) [42-44]. The given errors of the calculated bond distances originate from the EXAFSPAK algorithms. The given errors are the statistical ones and the true errors, including systematic ones, of the bond distances are usually a few times larger.

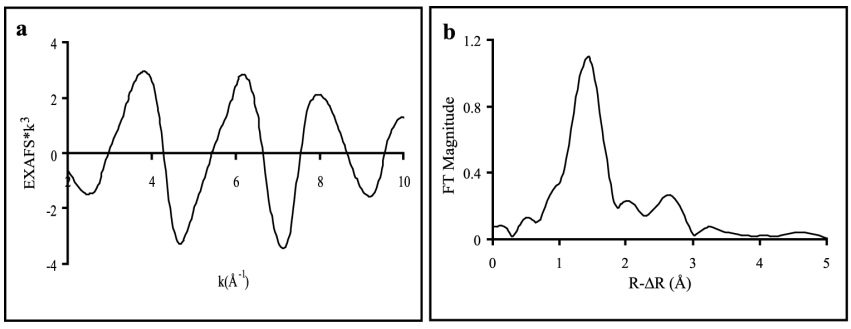

Figure 5. The k^3-weighted EXAFS function (a) and the Fourier transform (b).

Results and Discussion

Synthesis of Single-Source Precursors

In Paper **I**, the main objective was to access heterometallic complexes of late transition metals for the use as single-source precursors in materials production. Accessing heterometallic complexes of late transition metals *via* alkoxide complexes is not easy, due to low reactivity and low solubility of the complexes. We decided therefore to use an aminoalkoxide complex of nickel, supposedly more soluble in organic solvents and also much more reactive. Synthesis of the reactant (for further synthesis of heterometallic complexes), $Ni(\eta^2\text{-}OR^N)_2$ (R^N= $CHMeCH_2NMe_2$), was performed by a reaction between $[Ni(NH_3)_6]Cl_2$ and $NaOR^N$ in toluene, as described earlier [17]. However, this reaction produced the toluene clathrate and the solvent free complex was accessed by sublimation. Sublimation did not change the complex; toluene was released but bond angles and lengths, determined by single-crystal X-ray studies, remained practically the same, Figure 6 a.

Using the theory of hard and soft Lewis acids and bases, we concluded that a nickel aminoalcohol complex should react with a copper carboxylate complex [45]. The copper cation is a softer Lewis acid than the nickel cation and the aminoalkoxide ligand is a softer base than the carboxylate one - thus a possibility of reaching a heterometallic product *via* symmetrization. Further reaction of $Ni(\eta^2\text{-}OR^N)_2$ with $Cu(OCOC_2H_5)_2$ and $Cu(OAc)_2(H_2O)$ gave access to two heterometallic complexes. The first complex was studied by mass spectrometry and IR spectroscopy, but no single crystals were obtained. The studies concluded that the complex must have the formula $[CuNi_2(OCOC_2H_5)_3(OR^N)_3(R^NOH)]$. The structure of the second complex, Figure 6 b, $Ni(Ni_{0.25}Cu_{0.75})_2(\mu_3\text{-}OH)(\mu\text{-}OAc)(OAc)_2$ $(\mu,\eta^2\text{-}OR^N)_2(\eta^2\text{-}R^NOH)$, was determined by a single-crystal X-ray study.

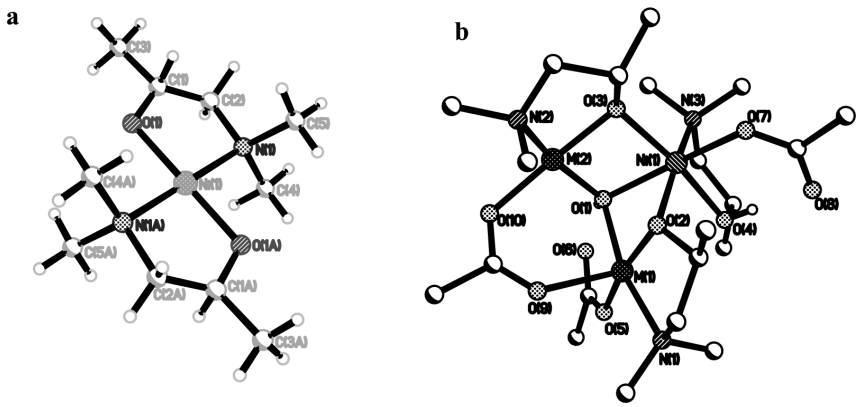

Figure 6. Molecular structure of $Ni(\eta^2\text{-}OR^N)_2$ (R^N= $CHMeCH_2NMe_2$) (a) and $Ni(Ni_{0.25}Cu_{0.75})_2(\mu_3\text{-}OH)(\mu\text{-}OAc)(OAc)_2(\mu,\eta^2\text{-}OR^N)_2(\eta^2\text{-}R^NOH)$, M(1) and M(2) are occupied by Cu 75% and Ni 25% (b).

The disorder in this complex, with an occupancy of 25% for Ni and 75% for Cu for two of the three metal atom positions, is a result of the synthesis process, where two different isomorphous complexes, $CuNi_2(\mu_3\text{-}OH)(\mu\text{-}OAc)(OAc)_2(\mu,\eta^2\text{-}OR^N)_2(\eta^2\text{-}R^NOH)$ and $Cu_2Ni(\mu_3\text{-}OH)(\mu\text{-}OAc)(OAc)_2(\mu,\eta^2\text{-}OR^N)_2(\eta^2\text{-}R^NOH)$, are formed giving an overall stoichiometry of 1:1 for Ni and Cu as indicated by the EDS analysis.

The main objective in Paper **II** was accessing heterometallic alkoxide complexes, as in **I**, suitable for oxide formation and zeolite implementation. Due to the unclear results of the heterometallic complexes in **I**, we decided to use a β-diketonate complex in **II**, hoping for better solubility and reactivity than with an alkoxide complex – and a better clarity of the structure of the complexes than with the aminoalcohol reactant. The complex used was $M^{II}(acac)_2$, M^{II}= Co, Ni, Zn or Mg and acac=$H_3CC(O)CHC(O)CH_3$. The manufacturer could not obtain totally water-free Ni and Co complexes and this turned out to be a major factor; the complexes have to be completely water-free in the reaction with $Ta(OMe)_5$ or $Nb(OMe)_5$, which were the two alkoxide complexes used. A test of the reaction between $Co(acac)_2$, used as provided from the manufacturer, and $Ta(OMe)_5$ resulted in hydrolysis of the latter. The hydrolysis provided MeOH and formation of $Co_4(acac)_6(OMe)_2(MeOH)_2$ and $Co(acac)_2{\cdot}2MeOH$, Figures 4 and 5 in **II**, respectively. Synthesis of $Co(acac)_2{\cdot}2MeOH$ can be reproduced by reaction of dry $Co(acac)_2$ and methanol, the yield is then practically quantitative. When dried, water-free $Co(acac)_2$ reacted with $Ta(OMe)_5$, no hydrolysis occurred and $Co_2Ta_2(acac)_2(OMe)_{12}$ precipitated practically quantitatively. Dried $Ni(acac)_2$, $Zn(acac)_2$, or $Mg(acac)_2$ reacted with $Ta(OMe)_5$ or $Nb(OMe)_5$ in the same manner as $Co(acac)_2$, and gave access to $M^{II}_2M^{V}_2(acac)_2(OMe)_{12}$, M^{II}= Co, Ni, Zn or Mg, and M^{V}= Ta or Nb, Figure 7. All the complexes are isostructural (monoclinic) and $Ni_2Ta_2(acac)_2(OMe)_{12}$ and $Zn_2Ta_2(acac)_2(OMe)_{12}$ are even isomorphous ($P2_1/c$) with $Co_2Ta_2(acac)_2(OMe)_{12}$, the only difference being the M^{II}-metal atom involved in the complexes (Table 1 in **II**). The smallest cell parameters of the three isomorphous complexes are for $Ni_2Ta_2(acac)_2(OMe)_{12}$ and the metal-oxygen bonds are the shortest ones in this complex too. This is in agreement with the smaller Ni(II) (ionic radii 0.690 Å) compared to the Co(II) (high-spin) and Zn(II), with almost equal size (ionic radii 0.745 Å and 0.74 Å, respectively).

A solution of the $Zn_2Ta_2(acac)_2(OMe)_{12}$ complex was studied by ^{1}H NMR and this made clear that the complex is intact in solution. The NMR spectrum showed three different signals corresponding to μ_3-OCH_3, μ-OCH_3, and terminal OCH_3, with the appropriate relation on integration (μ_3-OCH_3: μ-OCH_3: terminal OCH_3 = 1: 2: 3). However, when $Mg_2Ta_2(acac)_2(OMe)_{12}$ was studied by ^{1}H NMR (under the same conditions) no splitting of the μ_3-OCH_3 and μ-OCH_3 could be seen, probably due to the ionic nature of the magnesium-oxygen bonds in the complex. When the temperature was lowered, a broadening of the peak associated with the OCH_3 is seen, indicating a quick exchange of the OCH_3 groups in the complex at higher temperatures that is slowed down at low temperature, Figure 6 in **II**.

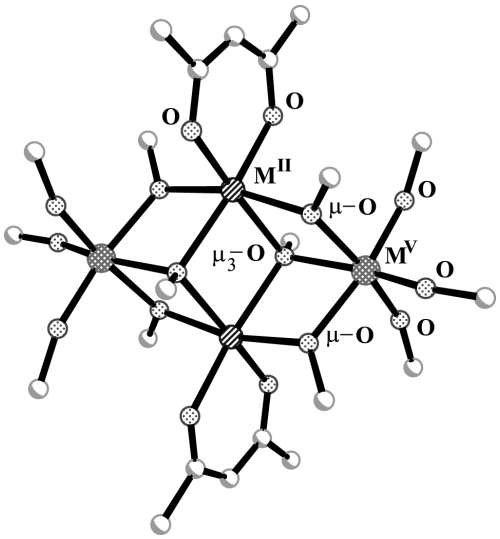

Figure 7. Molecular structure of $M^{II}_2M^{V}_2(acac)_2(OMe)_{12}$, M^{II}= Co, Ni, Zn or Mg and M^{V}= Ta or Nb , white circles are carbon atoms.

The importance of not adding any Lewis base to the reaction mixture is crucial. We accessed heterometallic complexes only when the starting material was water-free. Several attempts have been made to access heterometallic complexes [22-24] and they were successful only when the solvent was hydrocarbon based. If alcohol was added (acting as a Lewis base), the only result of the reaction was ligand exchange [25].

In order to use the synthetic strategy formulated with the syntheses of the heterometallic heteroleptic complexes $M^{II}_2M^{V}_2(acac)_2(OMe)_{12}$ in **II**, we used cobalt acetylacetonate in the reaction with molybdenum oxomethoxide, $MoO(OMe)_4$, in Paper **III**. These reactions use the β-diketonate metal complexes to provide stability in the solution (due to the chelating effects of the β-diketonate ligands) and the methoxide complexes to act as Lewis bases. The reaction was successful and provided $Co_2Mo_2O_2(acac)_2(OMe)_{10}$, Figure 8 a. Changing to nickel acetylacetonate instead of cobalt acetylacetonate in the reaction with $MoO(OMe)_4$ provided $Ni_2Mo_2O_2(acac)_2(OMe)_{10}$.

The new heterometallic molybdenum complexes have much lower solubility in toluene than the corresponding tantalum or niobium complexes. In order to improve the low solubility we altered the reaction by using $Ni(OR^N)_2$ (R^N= $CHMeCH_2NMe_2$) instead of $M^{II}(acac)_2$. This ligand-exchange reaction provided $Ni_2Mo_2O_2(OR^N)_2(OMe)_{10}$ and occurs when $Ni(L)_2$ (L=OR^N or acac) and $MoO(OMe)_4$ react in hexane. This complex was used to obtain xerogel powders, see Preparation of Oxide Materials below. Two new molybdenum complexes, containing the chelating ligands, were also produced as by-products. The structure of the complex containing the acac-ligand, $MoO(acac)(OMe)_3$, Figure 8 b, was determined by a single-crystal X-ray study.

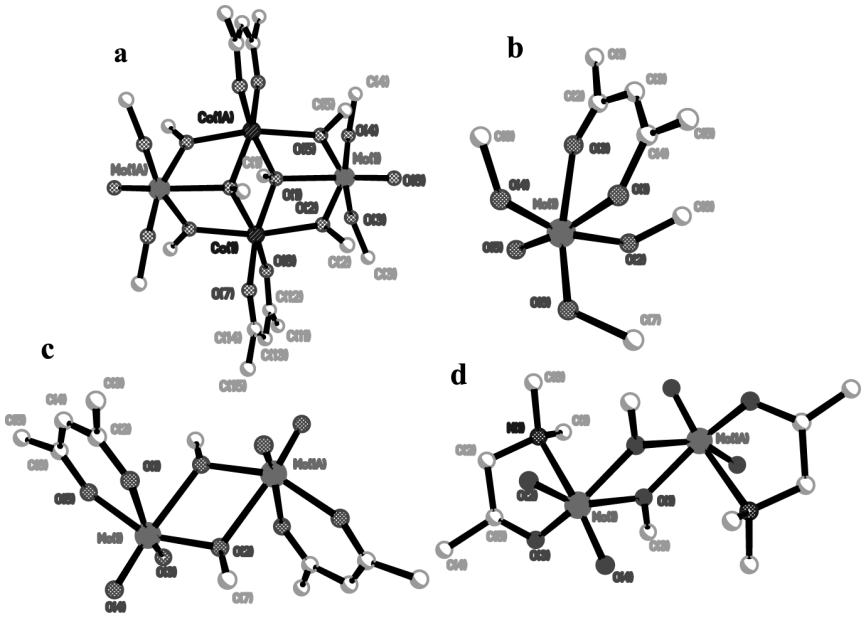

Figure 8. Molecular structures of $Co_2Mo_2O_2(acac)_2(OMe)_{10}$ (a), $MoO(acac)(OMe)_3$ (b), $[MoO_2(acac)(OMe)]_2$ (c) and $[MoO_2(OR^N)(OMe)]_2$ (d).

The by-product molybdenum complexes undergo ether elimination upon storage and the corresponding dioxo-complexes, $[MoO_2(L)(OMe)]_2$, were also isolated, Figure 8 c and d, respectively.

Single crystals of the two $Ni_2Mo_2O_2(L)_2(OMe)_{10}$ complexes, large enough for single-crystal X-ray studies, have not yet been possible to isolate. However, powder and a toluene/hexane solution of the complexes were studied by Ni-EXAFS. Cobalt and nickel atoms are of similar size, and therefore occupy approximately the same volume in a molecule, with nickel being the smaller one. The ionic radii of high spin Co(II) and Ni(II) in octahedral configuration are 0.745 Å and 0.690 Å, respectively [46]. Cobalt atoms have higher preference to octahedral angles in the inner-sphere than nickel. On the other hand, the distortion of the inner-sphere of a nickel atom can be severe and the O-Ni-O angles are shifted instead of differentiating the Ni-O bond lengths in the octahedron. Despite this difference in inner-sphere flexibility we propose the structure of $Co_2Nb_2(acac)_2(OMe)_{12}$, Figure 7, as a model compound for the description of the nickel-molybdenum complexes. Similarities in the results from the EXAFS experiment of the $Ni_2Mo_2O_2(L)_2(OMe)_{10}$ complexes indicate similarities in the molecular structures of these compounds, the nature of the chelating ligands being the only difference between them, Figure 9. The molecular structures of these heterometallic complexes are then analogous and follow well the model found in the X-ray single-crystal study – a tetranuclear complex belonging to the $Ti_4(OMe)_{16}$ structural type [47].

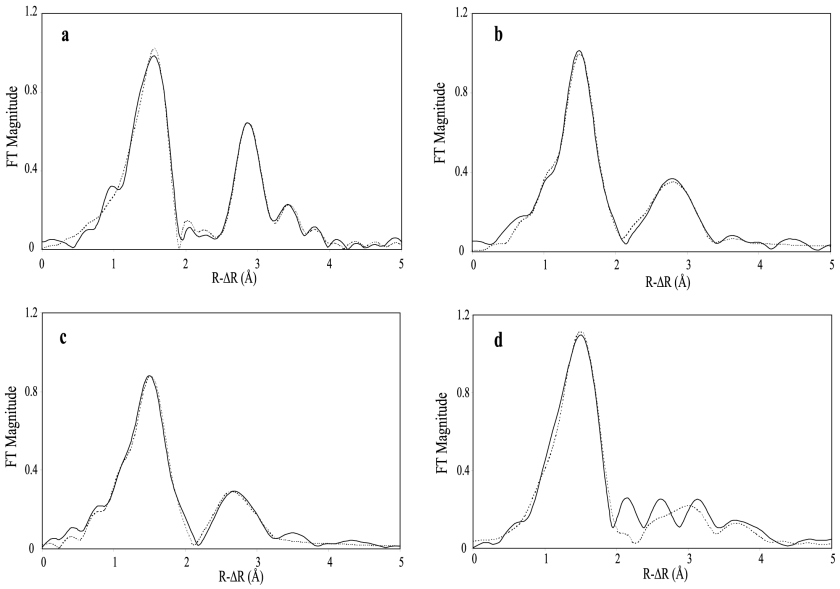

Figure 9. Fourier transforms (non-phase corrected) of $Ni_2Mo_2O_2(acac)_2(OMe)_{10}$ (a, powder), $Ni_2Mo_2O_2(OR^N)_2(OMe)_{10}$ (b, powder and c, solution) and $Co_2Nb_2(acac)_2(OMe)_{12}$ (d, powder). Solid lines experimental data and dotted lines calculated data.

The two chelating ligands used appear to play analogous structural roles leading to stabilization of the heterometallic $M_2M'_2X_{16}$ core, in both cases studied. The structure of the Co-Mo complex determined by X-ray single-crystal study was used successfully as a prototype for different Ni-Mo structures studied by EXAFS spectroscopy. For further use of these Ni-Mo complexes, a development of the synthesis procedures is important in order to obtain single-crystals for a complete structural determination and for easy handling in materials preparation.

Using the precursors synthesized and characterized in **II**, we wanted to explore the possibilities to produce mesoporous powders and dense films in Paper **V**. However, the toluene solutions of $M^{II}_2M^{V}_2(acac)_2(OMe)_{12}$, M^{II}=Co, Ni and M^{V}=Nb, Ta, were found to be extremely sensitive to hydrolysis with formation of poorly soluble homometallic acetylacetonate methoxides of the late transition metal, $[M^{II}(acac)(OMe)(MeOH)]_4$. We sought a way to increase the solubility and especially the stability of the heterometallic precursors in solution. An attractive step in this direction was to seek a possibility to produce derivatives with the same type of molecular structure but with longer alkyl chains of the alkoxide groups. This usually leads to decreased intermolecular interaction and higher affinity to hydrocarbon solvents. Application of tantalum ethoxide instead of tantalum methoxide in the reaction with cobalt and nickel acetylacetonates turned out to follow the predicted reaction pathway, and resulted in formation of the heterometallic acetylacetonate ethoxide complexes $M^{II}_2Ta_2(acac)_2(OEt)_{12}$, M^{II}=Co, Ni, Figure 10, with the desired 1:1 metal ratio.

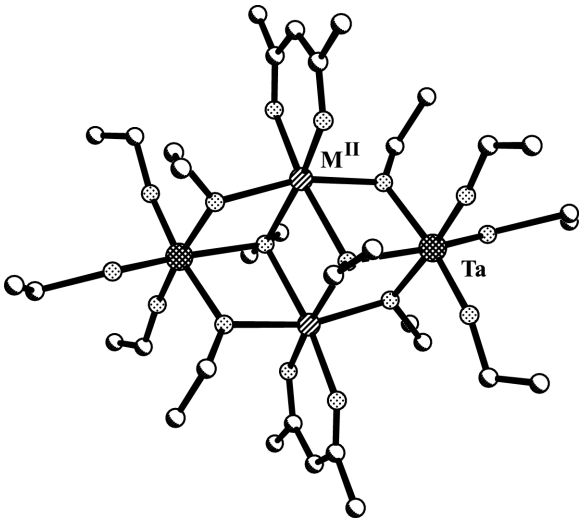

Figure 10. Molecular structure of $M^{II}_2Ta_2(acac)_2(OEt)_{12}$, M^{II}=Co, Ni, dotted circles are oxygen atoms and white circles are carbon atoms.

Additional advantages of the application of the liquid $Ta(OEt)_5$ instead of the solid $Ta(OMe)_5$ were in the higher solubility and the much higher reactivity with the acetylacetonates and, last but not least, much easier handling.

The two new ethoxide complexes crystallize in the triclinic space group P-1 (Table 1 in **V**), in contrast to the methoxide complexes with monoclinic space groups ($P2_1/c$ and C2/m) (Table 1 in **II**). The ethoxide groups are more disordered than the methoxide ones. This is a reflection of the larger size and lower metric symmetry of the ethyl groups, compared to the methyl ones. The titanium methoxide type, $Ti_4(OMe)_{16}$, appears to be a general feature of the vast majority of heterometallic alkoxide derivatives of primary alcohols.

Preparation of Oxide Materials

The low annealing temperature and easy handling makes the sol-gel technique a useful and attractive technique to obtain nanocomposite materials. In Paper **III**, $Ni_2Mo_2O_2(OR^N)_2(OMe)_{10}$ was used to obtain xerogel powders. The hydrolyzed complex was annealed at four different temperatures. Powder X-ray diffraction of the xerogel shows incipient crystallization of $NiMoO_4$ [16-0291][48] at 400 °C, Figure 5 in **III**. At 700 °C, the crystallization of the monoclinic (P2/c) oxide $NiMoO_4$ was more pronounced and another monoclinic (I2/m) $NiMoO_4$ phase [33-0948][48] was seen as well. SEM of the annealed xerogels confirmed the results from the powder X-ray diffraction analysis. At 300 °C, the gel was porous with a low degree of crystallinity and no sharp edges on the grains could be seen, Figure 11 a. Annealing at 400 °C started the crystallization and the grains became larger, but they were still porous, Figure 11 b.

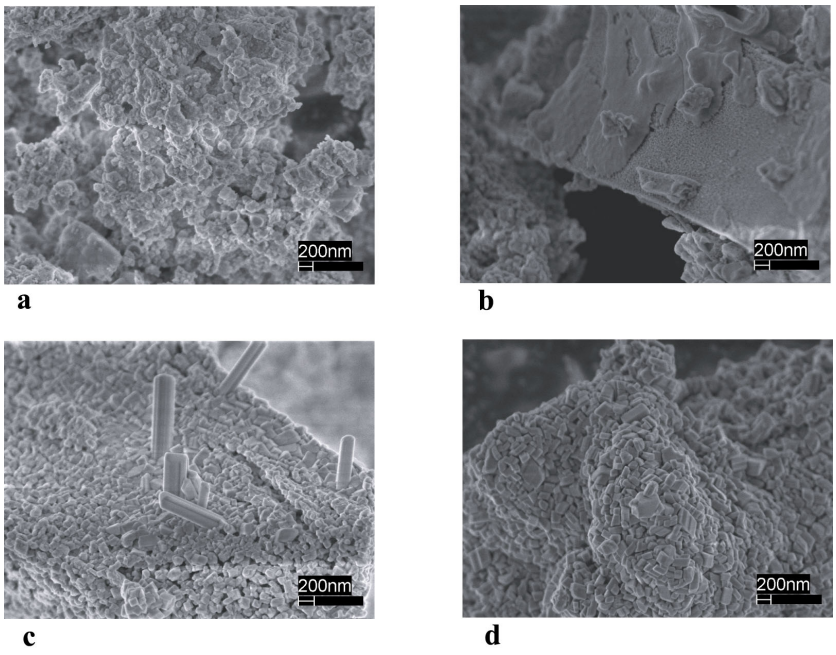

Figure 11. SEM images of the xerogel from $Ni_2Mo_2O_2(OR^N)_2(OMe)_{10}$ annealed at different temperatures, 300 °C (a), 400 °C (b), 500 °C (c) and 700 °C (d).

The crystallization process was well on its way at 500 °C – the grains were uniform in size, 75-100 nm, and well packed but with a large surface area, Figure 11 c. Small rods of crystallized oxide could be seen. At 700 °C, the grains were even larger, 175-250 nm, Figure 11 d, and rods, with a diameter of 1 µm, of the crystallized oxide grains were uniformly spread over the sample. The grains were well packed with low porosity and the grain size provides a large surface area, thus a material well suited for catalysis experiments.

The preparation of oxide material from the new nickel-molybdenum aminoalcohol complex was successful, with materials annealed at 500 °C showing uniform grain size and a large surface area.

Producing mesoporous powders from the precursors synthesized in Paper **II** and the new precursors synthesized in Paper **V** was one of the goals in **V**. Powder X-ray diffractograms from five oxide powders are shown in Figure 6 in **V**. The diffractograms indicate that the two oxide powders from $Co_2Ta_2(acac)_2(OMe)_{12}$, (a and b) are crystalline. The powder annealed at 800 °C for 2 h has more distinct features than the one treated at 650 °C for 4 h. Two different oxides have been detected in the 800 °C sample: $CoTa_2O_6$ [32-0314] [48] and Co_3O_4 [42-1467] [48]. These two oxides were also detected in the sample annealed at 650 °C but the peaks were small and non-distinct and the result was therefore less certain. For the powders obtained from $Co_2Ta_2(acac)_2(OEt)_{12}$ (d and e), the peaks were broader and less distinctly shaped than the peaks from the methoxide samples. The same phases can, however, be detected for the samples prepared at the same

temperatures, indicating an analogy in the chemical transformations and crystallization behaviour, but smaller particle size and lower degree of crystallinity with the powders from the ethoxide samples. This is in agreement with the earlier observed trend for titanates with different size of the ligands [21]. Also for the powder from $Ni_2Ta_2(acac)_2(OMe)_{12}$, annealed at 650 °C for 4 h, two different oxides were detected: $NiTa_2O_6$ [32-0702] [48] and NiO [44-1159] [48], Figure 6 c in **V**. The nickel oxide is stable to oxidation in air on heating and remained therefore in this form (NiO instead of Ni_3O_4, as for the cobalt oxide above) in the annealed samples. Samples heat-treated at lower temperature (at 300 and 400 °C) were amorphous after annealing and at 500 °C broad peaks in the diffractograms indicated incipient crystallization and short-range ordering in the sample, in agreement with the detected peaks in the fully crystallized samples.

SEM images of the oxide powders obtained from $Co_2Ta_2(acac)_2(OMe)_{12}$ at 650 °C and 800 °C show dense and well-faceted xerogel particles with an even size distribution; the particles are 30-35×45-55 μm in size, Figure 12. Small islands of a crystallized oxide phase can be seen on the surface of the xerogel particles. These oxide grains are much smaller, 1-3 μm in diameter, and very well faceted. In contrast to the dense xerogel particles from $Co_2Ta_2(acac)_2(OMe)_{12}$, the xerogel from $Ni_2Ta_2(acac)_2(OMe)_{12}$ have a very porous structure, making it very difficult to obtain good SEM images of the xerogel particles. It is not well faceted and smaller (25×35 μm) compared to the xerogel obtained from $Co_2Ta_2(acac)_2(OMe)_{12}$. The two precursors ($Co_2Ta_2(acac)_2(OMe)_{12}$ and $Ni_2Ta_2(acac)_2(OMe)_{12}$) have been hydrolyzed and heat-treated in the same manner, indicating that the difference in morphology can be attributed to differences in hydrolysis and crystallization for the nickel and cobalt compounds.

TEM images of typical particles of the oxides prepared from the $Co_2Ta_2(acac)_2(OMe)_{12}$ precursor, followed by thermal annealing at 800°C, show large dark particles and small agglomerates, Figure 13 a. Selected Area Diffraction (SAD) on the small particles, Figure 13 b, revealed a pure $CoTa_2O_6$ polycrystalline phase. High-resolution TEM and SAD analysis on the large particle, Figure 13 c and d, showed presence of a monocrystalline Co_3O_4 phase, probably doped with tantalum cations. This phase preserves the *fcc* structure but with smaller parameter of about 8.0 Å instead of 8.17 Å for pure Co_3O_4. These observations are consistent with the powder X-ray diffraction patterns and with EDS analysis, Figure S2 in **V**, which showed the ratio Co:Ta to be 1:2, Figure S2 a, for the polycrystalline particles and a majority of cobalt for the monocrystalline grains, Figure S2 b.

TEM and HRTEM images of the oxide prepared from the $Co_2Ta_2(acac)_2(OMe)_{12}$ precursor, followed by thermal annealing at 650°C, shows both amorphous and crystalline oxides, Figure 9 in **V**, which is consistent with the powder X-ray analysis. TEM image on the amorphous zone evidenced the presence of well-organized mesopores in the oxide grains, Figure 9 a in **V**. HRTEM image of the crystalline parts showed the expected $CoTa_2O_6$ phase in agreement with the XRD analysis, Figure 9 b in **V**. Surface area determination (BET measurement) confirmed the presence of mesopores of 4 nm in diameter, which also were observed with TEM, but with a low surface area (10 m^2/g) and no microporosity.

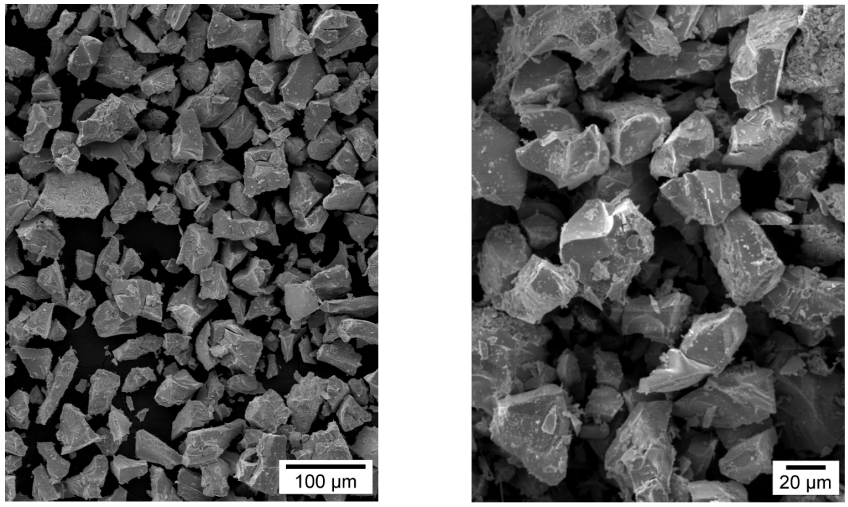

Figure 12. SEM images of oxide powders from $Co_2Ta_2(acac)_2(OMe)_{12}$, annealed at 800 °C for 2 h (a) and at 650 °C for 4 h (b).

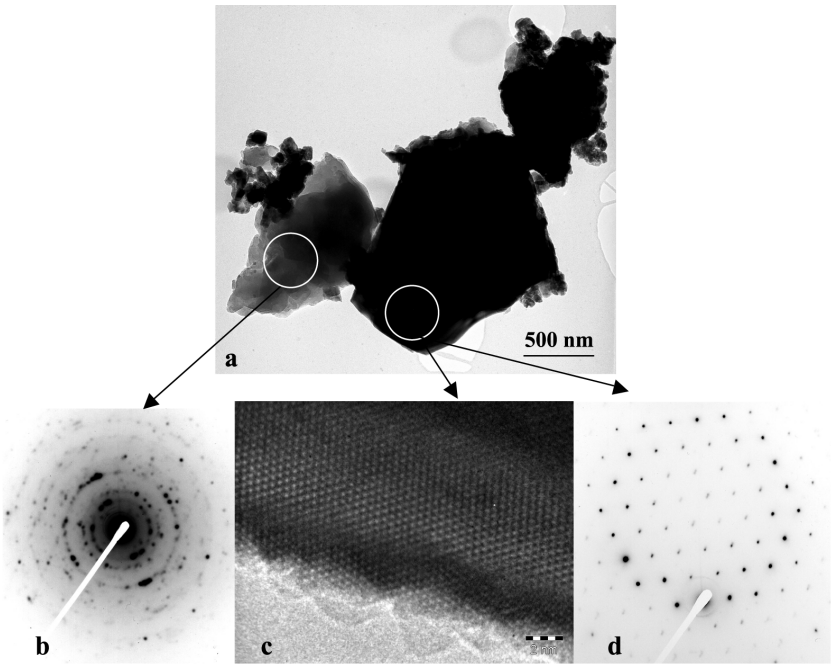

Figure 13. TEM of the oxide obtained from $Co_2Ta_2(acac)_2(OMe)_{12}$ at 800°C, showing typical oxide particles (a), SAD of the polycrystalline $CoTa_2O_6$ grain (b) and HRTEM and SAD of the monocrystalline Co_3O_4 (zone axis [110]) (c and d).

The second goal in **V** was to test the precursors from **II** and **V** for film making by spin-coating on two different substrates, Si and SiO_2. The deposition on the substrates was performed by applying solutions of the precursors in toluene, a solvent usually not applied in pure sol-gel preparation of coatings. The common practice recommends application of polar solvents such as alcohols or functional alcohols (alcohols with an extra functional group such as a methoxide group in *e.g.* 2-methoxyethanol) in order to achieve good coverage of the substrates (most often hydrophilic metal oxides such as SiO_2 or Al_2O_3) and good affinity of the solutions to them. Solutions of precursors in toluene can be applied successfully for this purpose – the films were very smooth and well defined on both substrates, independently of concentration and number of layers. The films on SiO_2 display some cracks and blisters to a somewhat larger extent than those on Si. This is probably due to thermal mismatch between the SiO_2-substrate and the newly formed oxide film.

Characterization of the oxide films on SiO_2-substrate by powder X-ray diffraction was not possible because of large absorption of the radiation due to surface roughness of the substrate. Characterization of the oxide films on Si-substrate was carried out with XRD without any problems. In the X-ray pattern of the films heat-treated at lower temperatures (650 ºC), features from the substrate surface remained noticeable (*e.g*. the peak near 34 º is originating from the Si[110], Figure 3 d in **V**) This is probably due to a lower crystallinity and own reflectivity of the film. In the oxide film from 4 layers of 0.20 M of $Co_2Ta_2(acac)_2(OEt)_{12}$ with 4 h annealing at 650 °C, $CoTa_2O_6$ [32-0314] [48] was detected, Figure 3 c in **V**. After annealing at higher temperature (800 °C) but shorter time (2 h) the oxide film from 5 layers of 0.14 M of $Co_2Ta_2(acac)_2(OMe)_{12}$ had crystallized even better, with two different phases detected by XRD: $CoTa_2O_6$ [32-0314] [48] and a start of the crystallization of Co_2O_3 [42-1467] [48], Figure 3 d in **V**.

SEM images of the oxide films revealed smooth and evenly distributed films on the substrates, Figure 14. It was not possible to detect the different layers, which indicates that the depositions were uniform. The thickness of the films was determined from the SEM images and varied with number of applied layers. Figure 14 shows two images of oxide films at the edge of the substrates and these were used for determining the thickness of the films. Six layers, Figure 14 a, and four layers, Figure 14 b, of 0.20 M $Co_2Ta_2(acac)_2(OEt)_{12}$ on Si resulted in oxide films with the thickness of 0.50 μm.

However, three layers on two Si substrates also resulted in 0.50 μm thick oxide films, independent of solution concentration (0.20 M or 0.28 M of $Co_2Ta_2(acac)_2(OEt)_{12}$). Three layers of deposition on SiO_2 resulted in a 0.26 μm thick oxide film from a 0.20 M solution of $Co_2Ta_2(acac)_2(OEt)_{12}$ and a 0.37 μm thick one from a 0.28 M solution, indicating a possible small dependence of number of layers, concentration and thickness of the film.

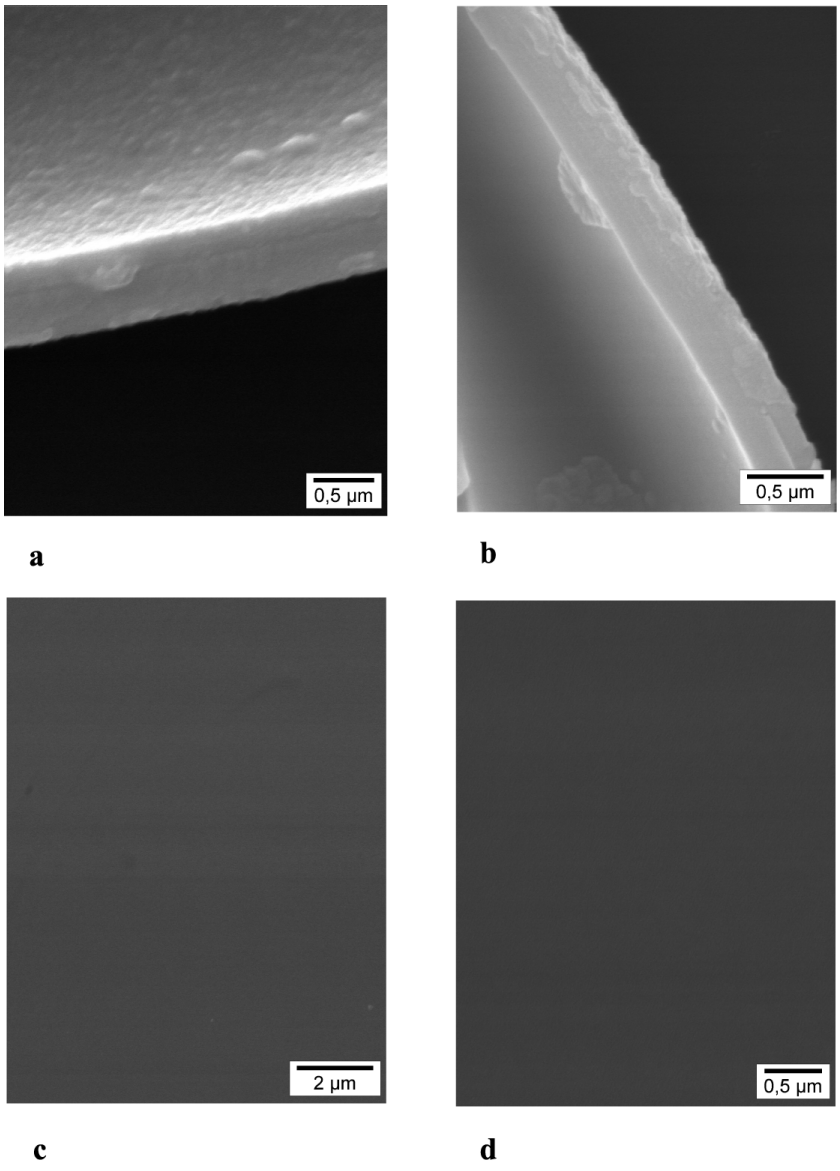

Figure 14. SEM images of oxide films obtained from 0.20 M $Co_2Ta_2(acac)_2(OEt)_{12}$,used for thickness determination, 6 layers on Si (650 °C for 4 h) (a) and 4 layers on Si (650 °C for 4 h) (b). SEM images of oxide films obtained from 0.20 M $Co_2Ta_2(acac)_2(OEt)_{12}$, 4 layers on SiO_2 (550°C for 2 h) (c) and 3 layers on Si (650 °C for 4 h) (d).

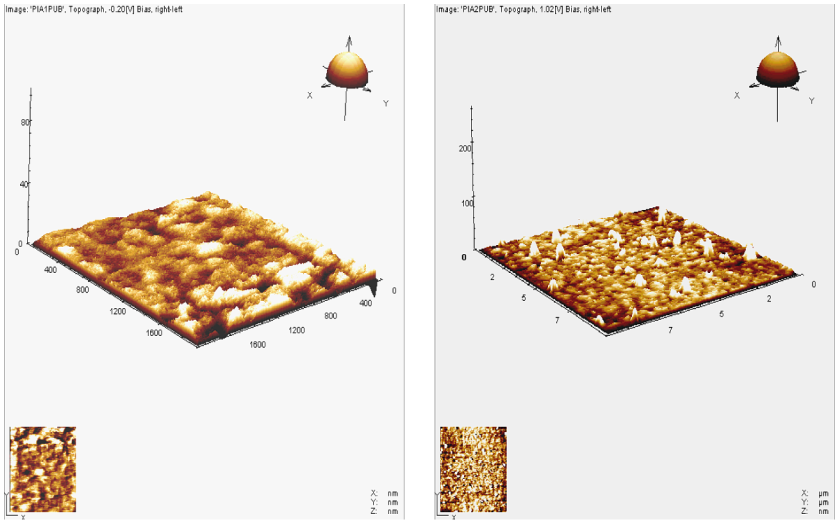

a **b**

Figure 15. AFM images of oxide films obtained from 3 layers of 0.28 M $Co_2Ta_2(acac)_2(OEt)_{12}$ (650 °C for 4 h) (a) and 6 layers of 0.20 M $Co_2Ta_2(acac)_2(OEt)_{12}$ (650 °C for 4 h) (b).

Atomic force microscopy (AFM) analysis of the oxide films on Si-substrate showed that the surface was smooth and the root mean square roughness was 2.4 nm for a three-layer oxide film made from a 0.28 M solution of $Co_2Ta_2(acac)_2(OEt)_{12}$, Figure 15 a, and 4.0 nm for an oxide film with 6 layers of 0.20 M $Co_2Ta_2(acac)_2(OEt)_{12}$, Figure 15 b.

Nanopowders and oxide films were possible to produce successfully with the new class of heterometallic heteroleptic alkoxides $M^{II}_2Ta_2(acac)_2(OR)_{12}$, M^{II}=Co, Ni, R=Me, Et, with well-defined structure at a relatively low temperature and short sintering time. Toluene proved to be a very good solvent to use.

Zeolite Implementation

Hydrolysis and zeolite implementation of the $M^{II}_2M^{V}_2(acac)_2(OMe)_{12}$ complexes, described in Paper **II**, were the main goals of Paper **IV**. EXAFS analysis of the solid complex ($Co_2Nb_2(acac)_2(OMe)_{12}$) and a solution of it in toluene confirmed that the complex remained intact in solution; the Co-O distances remained almost the same, 2.02(2) Å and 1.98(2) Å for the solid, Figure 16 a, and the solution sample, Figure 16 b, respectively, compared to 2.083(4) Å for the Co-μ-O bond and 2.031(4) Å for the Co-acac-O bond in the single-crystal X-ray determination of the complex. Hydrolysis was carried out and produced a viscous sol. The sol gelled and dried on evaporation, leaving a fine powder. TG analysis showed three distinct steps at 120 °C, 390 °C, and at 480 °C. SEM-EDS analysis revealed uniform distribution of the metals in the powder, probably due to too small particles. Powder X-ray diffraction revealed only an amorphous phase from

powder heated to 500 °C, but a crystalline oxide from powder heated to 900 °C. This oxide consisted of an equimolar mixture of $CoTa_2O_6$ [32-0314] [48] and $Co_4Ta_2O_9$ [38-1461] [48]. EXAFS analyses of non-heat-treated and heat-treated hydrolysis product (to 500 °C) revealed that the coordination sphere around the Co atoms remained intact after heat treatment, Co-O distances are 1.98(2) Å, Figure 16 c, and 1.94(2) Å, Figure 16 d.

The acetylacetonate rings should be present in the non-heat-treated sample but Co-C distances are not seen in the FT spectrum of the hydrolysis product, Figure 16 c. This may be an indication of disorder of the carbon atoms in the rings.

Hydrolysis occurred in the same manner for $Co_2Ta_2(acac)_2(OMe)_{12}$, $Co_2Nb_2(acac)_2(OMe)_{12}$, and $Ni_2Ta_2(acac)_2(OMe)_{12}$.

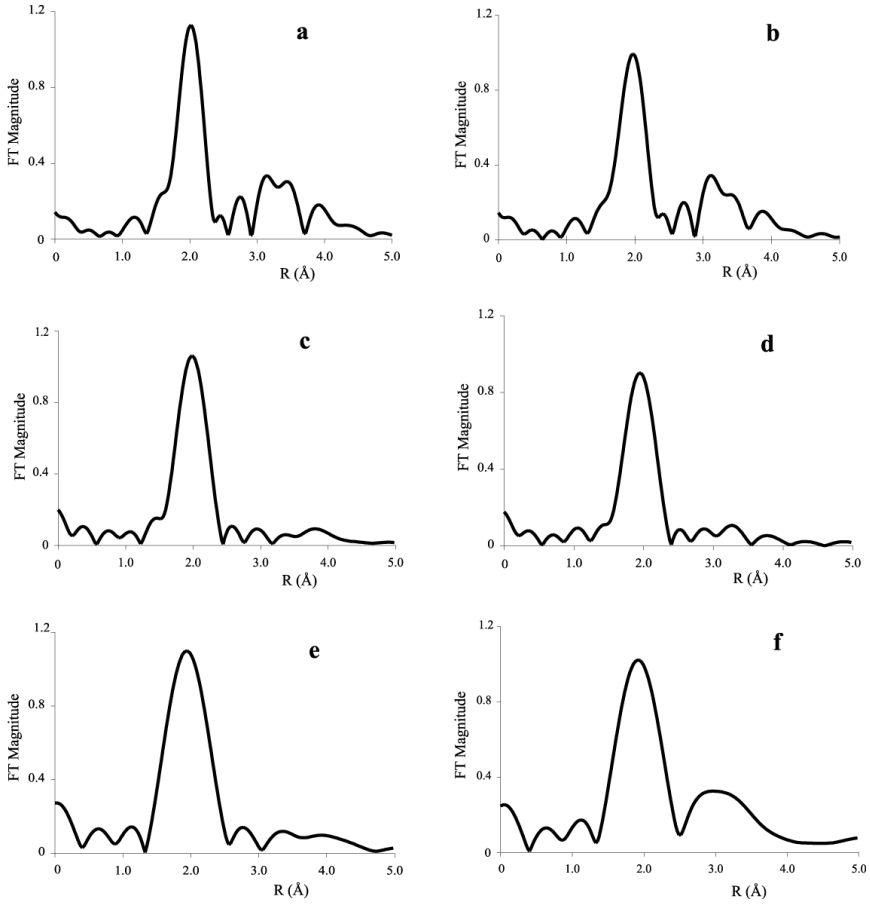

Figure 16. Phase corrected Fourier Transforms of the different EXAFS analyses of $Co_2Nb_2(acac)_2(OMe)_{12}$ powder (a), solution (b), non-heated bulk hydrolysis product (c), heated bulk hydrolysis product (d), non-heated nanocomposite (e) and heated nanocomposite (f).

When a toluene solution of $Co_2Ta_2(acac)_2(OMe)_{12}$ (purple in colour – *i.e.* octahedral coordination of the Co – though often more red or pink; the tetrahedral one is blue) was added to dry 12 Å NaY zeolite, an exothermic reaction took place and the zeolite solution changed colour into ice blue. After evaporation of the solvent, the dry solid was still its original white, indicating that the complex was implemented into the cavities of the zeolite. The FT spectrum of a zeolite sample heated to 500 °C (made from $Co_2Nb_2(acac)_2(OMe)_{12}$, the implementation occurred in the same way as for $Co_2Ta_2(acac)_2(OMe)_{12}$), showed a new feature, Figure 16 f, compared to the non-heat-treated zeolite sample, Figure 16 e, This feature was interpreted as interactions between the oxide (produced when heating the complex) and Si atoms of the zeolite. These distances are 2.96(3) Å, *i.e.* in the same range as a Co-(O)-Si bond is. The coordination sphere around the Co atoms remains intact with Co-O distances of 1.94(2) Å and 1.92(2) Å. We tested implementation with another zeolite (3 Å NaA zeolite) and all other conditions the same. No reaction took place, not even after heating the reaction sample. It is an indication that 12 Å cavities are crucial for implementation to take place.

The catalytical activity was tested by the reaction of complete oxidation of methanol in gas phase [49]. Dimethyl ether, H_2O and CO_2 were the main reaction products; formation of CO was not detected. A 98%-conversion of methanol into CO_2 and H_2O was observed at 90°C over the obtained nanocomposite catalyst, with only traces of dimethyl ether. It is a high activity for the Co-Ta-NaY oxide nanocomposite catalyst with a rather low content of the catalytically active component in the substrate (5%). It is especially interesting to note that the pure NaY zeolite only caused formation of dimethyl ether under the same conditions.

Implementation of $Co_2Nb_2(acac)_2(OMe)_{12}$) into 12 Å NaY zeolite was tested again in Paper **VI**, with both room temperature zeolite and cooled one, in order to try to slow down the infiltration of the metal complex. We obtained the same results with both room temperature and cooled zeolite – the zeolite-complex solution turned ice blue immediately when the solution was added. After cooling of the warm solution, the toluene was evaporated off and the implemented zeolite turned out, after drying, to still to be white, supporting the idea that the coloured centres were located inside the pores of the zeolite. EXAFS-analyses were performed on both non-heat-treated zeolite nanocomposite and on heat-treated nanocomposite (400 °C for 1 h), Figure 17. The heat-treated sample showed that the complex has been destroyed, with transfer of the Co-atoms inside the smaller channels of the zeolite, due to new Co-Si distance, 3.523(6) Å, Figure 17 d, not shown by the non-heat-treated sample, Figure 17 b. The coordination around the cobalt atoms is almost the same; the data fitting of the EXAFS analysis show Co-O distances of 2.039(4) Å and 1.992(3) Å in the non-heat-treated and the heat-treated nanocomposite, respectively. Niobium-EXAFS of the zeolite nanocomposite showed the Nb-atoms to be octahedrally surrounded by oxygen atoms with a great degree of disorder, especially in the heat-treated sample. The highly charged niobium cations are supposedly locked in the larger 12 Å pores, having difficulties to move by diffusion. This results in disordered coordination inside the pores.

The decomposition of the oxohydroxide complex, formed initially under further heat-treatment, with transfer of the cobalt atoms into the rectangular channels of the zeolite Y, should be possible to model by using silsesquioxane complexes. This led to the idea to investigate the interaction of the same alkoxide complex with a cyclohexylsilsesquioxane ligand, proposed earlier as a good model for reconstruction of implemented zeolite structures [50-63].

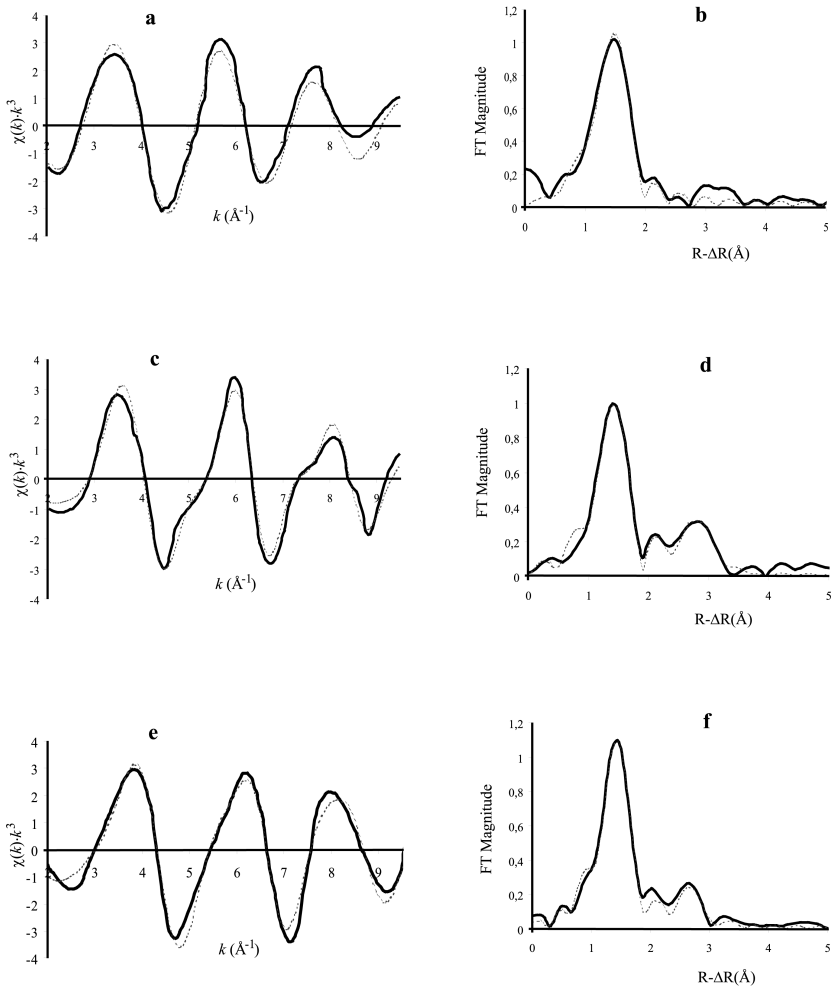

Figure 17. EXAFS functions and Fourier Transforms (non-phase corrected) of non-heat-treated Co-nanocomposite (a and b), heat-treated Co-nanocomposite (c and d) and $Co[(C_6H_{11})_7Si_7O_{12}]_2H_4$ (e and f), solid line experimental data and dashed line calculated data.

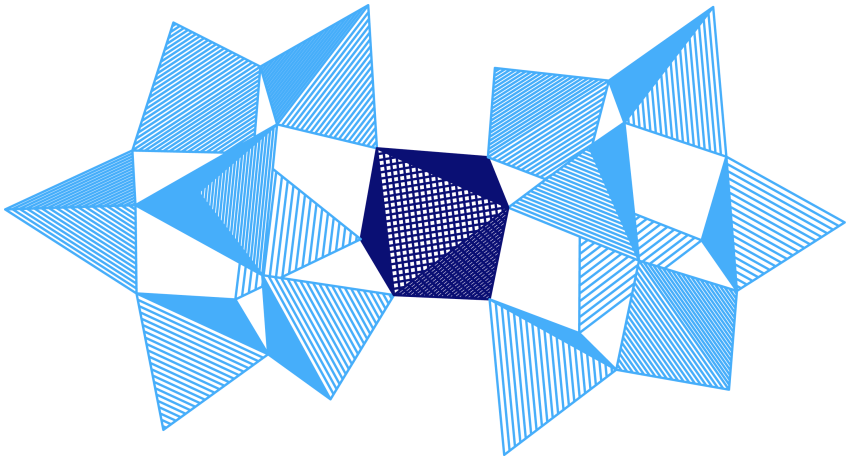

Figure 18. Polyhedral model of $Co[(C_6H_{11})_7Si_7O_{12}]_2H_4$ with the Co-O octahedron in the centre (dark blue) and the ring formations of the Si-O tetrahedra connecting to the Co-O octahedron (light blue).

The reaction between $Co_2Nb_2(acac)_2(OMe)_{12}$ and the cyclohexylsilsesquioxane resulted in a new metallasilsesquioxane complex, $Co[(C_6H_{11})_7Si_7O_{12}]_2H_4$, Figure 18. The complex is formed according to the following reaction:

$$Co_2Nb_2(acac)_2(OMe)_{12} + 4\ (C_6H_{11})_7Si_7O_9(OH)_3 \rightarrow 2\ Co[(C_6H_{11})_7Si_7O_{12}]_2H_4 + \\ + 2\ Nb(acac)(OMe)_4 + 4\ MeOH$$

It was isolated in high yield (79%) as pinkish violet crystals. The structure of $Co[(C_6H_{11})_7Si_7O_{12}]_2H_4$ is built up by a two cubes of the silsesquioxanes ligands, connecting to the cobalt centre *via* oxygen atoms. The coordination around the cobalt atom is a distorted octahedron, with Co-O distances of 1.877(2)-2.208(3) Å. The Co-Si distances are 3.487(2)-3.576(4) Å to the closest Si-atoms. Due to twinning problems, the single-crystal X-ray study was impossible to complete, but a preliminary model has been obtained with space group Pn. Data fitting of the EXAFS analysis, Figure 17 e, show one Co-O distance, 1.957(3) Å and one Co-Si distance, 3.387(8) Å, Figure 17 f, which is in very good agreement with the obtained single-crystal model (as the EXAFS analysis cannot detect the distortion of the cobalt-oxygen octahedron nor the small changes in the Co-Si distances).

According to the very similar Fourier Transformations of the EXAFS analyses of the heat-treated Co-nanocomposite and the Co-silsesquioxane complex, Figure 17 d and f, respectively, the metallasilsesquioxane complex can serve as a NaY zeolite analogue with implemented metal atoms – demonstrating the success of the molecular model approach.

Concluding Remarks

In order to be successful with sol-gel preparation of nanocomposite materials it is important to know what to start with in the synthesis you want to perform, so that you obtain the single-source precursor (SSP) desired. You also need to know the different synthesis pathways available, to be able to choose the correct one. When the SSP has crystallized, characterization must be performed with several different techniques, *e.g.* X-ray, IR, NMR and EXAFS.

All the materials prepared, whether they are nanocomposite powders or thin films, need to be characterized. SEM and TEM analyses are used to determine the composition, particle size, and thickness and smoothness of the films, for a detailed characterization of the materials.

The work described in the thesis has provided me with a growing understanding of how to approach different problems with materials preparation in the future, from the start with synthesis of the SSP to the characterization of the desired product.

The main conclusions of the work presented in the thesis are

- The approach based on Lewis acid-base interactions turned out to be successful. The reaction of a M^{II} β-diketonate complex with a Lewis base M^{V} alkoxide provided different heteroleptic heterometallic complexes, suitable as SSPs for materials production. A series of complexes with isomorphous structures were obtained, making the prediction of the structure of the complexes straightforward.

- The titanium methoxide, $Ti_4(OMe)_{16}$, structure type, appears to be a general feature of heterometallic alkoxide derivatives of primary alcohols.

- Nanopowders and oxide films were successfully produced with the new class of alkoxides, $M^{II}_2Ta_2(acac)_2(OR)_{12}$ M^{II}=Co, Ni and R=Me, Et, with well-defined structure obtained at a relatively low temperature and short sintering time. The nanopowders from $Ni_2Mo_2O_2(OR^N)_2(OMe)_{10}$ are well packed with low porosity and large surface area; well suited for catalysis experiments.

- Toluene has turned out to be a very good solvent to use in synthesis and materials production.

- Hydrolysis and implementation of the complexes into 12 Å NaY zeolites of the complexes provided nanocomposite materials with catalytical properties and a specific affinity of the complexes with the 12 Å zeolite. The synthesized metallasilsesquioxane complex can serve as a zeolite Y analogue with implemented metal atom, making it suitable as a model complex for further studies of the implemented zeolite complexes.

Svensk sammanfattning

Avhandlingen behandlar alkoxider och alkoxidderivat och deras möjligheter att vara utgångsämnen i materialframställning för ytbeläggning och katalys. Idag behövs nya material till t.ex. ytbeläggning så att ytan tål väder och vind eller gör den mindre repkänslig. För att omvandla billiga utgångsämnen till bra startmaterial för syntes av plaster och läkemedel behövs katalysatorer. De gör att reaktionerna sker snabbare och ofta vid en lägre temperatur än utan katalysator. Katalysatorerna är ofta metalloxider med varierande sammansättning. Då träsprit (metanol) omvandlas till formaldehyd används en järnmolybdenkatalysator och när växtfetter omvandlas till margarin används en nickelbaserad katalysator. I dagens bilar används en rodiumplatinakatalysator för att omvandla kolmonoxid, kväveoxid och kolväten till koldioxid, kvävgas och vattenånga. Platina och rodium finns inte i obegränsade mängder och ett av målen med katalysatorforskningen är att få fram ett alternativ till dagens bilkatalysatorer. Ett annat mål är att få katalysatorn att fungera vid lägre temperatur än rodiumplatinakatalysatorn som behöver bli riktigt varm, ca 190 °C, för att fungera bra. Under uppvärmningstiden sker ingen omvandling av avgaserna.

Målet med mitt doktorandarbete har varit att få fram startmaterial som kan omvandlas till katalysatorer eller bli bra ytbeläggningsmaterial, helst vid lägre temperatur än vad som behövs idag. Startmaterialen ska vara lätta att syntetisera, upprena och ha en bestämd sammansättning. Jag har arbetat med heteroleptiska (med olika typer av ligander) heterometalliska (med två olika metaller) alkoxider. Metallalkoxider $(M(OR)_n)_m$ är ämnen med en eller flera metallatomer (M) med alkoxidgrupper (OR) bundna till sig. Alkoxidgrupperna kommer från olika sorters alkoholer (R varierar, t.ex. är $R=CH_2CH_3$ i vanlig sprit, etanol CH_3CH_2OH). De binder in till metallatomen via syreatomen. Alkoxider används därför att de är ganska lätta att syntetisera och vid värmebehandling avgår kolvätedelen vid låg temperatur och en metalloxid blir kvar. Metalloxiden kan utgöra katalysatorn om man valt lämplig metallatom från början eller kan man använda alkoxiden vid ytbeläggning och sedan värmebehandla ytan. Då bildas ett skyddande oxidlager direkt på ytan. Ett problem med alkoxider som startmaterial är att det finns ganska få alkoxider med bestämd struktur, speciellt om man vill ha två sorters metallatomer i komplexet.

De tre första artiklarna från mitt doktorandarbete (**I**, **II** och **III**) har som utgångspunkt att syntetisera utgångsämnen med bestämd sammansättning och struktur. I artikel **II** har vi fått fram en ny klass av heteroleptiska heterometalliska alkoxider. Vi syntetiserade fem olika komplex där ingående metallatomer varierade och vi kan se att samtliga i klassen har liknande egenskaper. Vi fick stort utbyte i de synteserna och komplexens strukturer var väldefinierade. I artikel **I** användes en annan sorts ligand än i artikel **II**. Det visade sig att de komplexen hade svårbestämda strukturer och vi fick ganska låga utbyten. Artikel **III** beskriver liknande syntes som i artikel **II** men med molybden istället för tantal och niob. Molybdenkomplexen har mycket sämre löslighet än de med tantal och niob. Detta gjorde att ett byte av ligand verkade intressant för att öka lösligheten. Syntesen

med ett aminoalkohol komplex ($Ni(OR^N)_2$, R^N= $CHMeCH_2NMe_2$) resulterade i ett nickelmolybden-komplex med högre löslighet, som förväntat.

I artiklarna **III**, **IV** och **V** har vi använt de nya komplexen för att framställa oxidmaterial. Komplexen har testats för dels ytbeläggning och dels för framställning av nanokompositpulver. De erhållna ytorna är mycket jämna och utan att de olika lagren syns och ytbeläggningen har hög densitet. Hög densitet hos ytbeläggningar baserade på rena alkoxidkomplex är svårt att få då hydrolys- och kondensationsstegen, som ger det sammanhängande lagret, ofta sker för snabbt och lagren blir ojämna och med sprickbildning. Nanokompositpulver (med två eller flera faser med välbestämda sammansättningar) framställdes för katalysreaktion och via analyser såg vi att de är porösa, vilket är en förutsättning för effektiva katalysreaktioner – ju större yta desto fler reaktionsplatser. Vi utökade dessutom den nya klassen av heteroleptiska heterometalliska alkoxider med syntes och strukturbestämning av utgångsämnen med etoxidligander istället för som tidigare metoxidligander. Denna förändring visade sig underlätta dels syntesen dels uppreningen av utgångsmaterialet.

I artikel **IV** har vi använt de nya utgångsmaterialen för att testa den katalytiska förmågan. Zeoliter implementerade med utgångsämnen med kobolt och niob testades för oxidation av metanol och det visade sig att den nya katalysatorn är effektiv. Fortsatt analys av zeoliter har vi beskrivit i artikel **VI**. Det som intresserar oss är att undersöka hur komplexet sitter fast i zeolitens tunnlar och hur mycket komplex man kan ”ladda” zeoliten med för att få en effektiv katalysator. Då zeoliter är stora nätverk av aluminiumsilikater med komplicerad struktur kan man använda silsesquioxaner som en enklare modell av zeoliter (artikel **VI**). Den silsesquioxan som använts består också av aluminiumsilikat men är mycket mindre och med bestämd struktur. Utgångsämnet hakade fast i två silsesquioxaner och strukturen av detta komplex har bestämts. När silsesquioxan-komplexet jämfördes med zeolit-komplexet i en analys såg man att de hade samma typ av bindningar mellan metallatomerna och nätverket. Detta gör att man kan studera silsesquioxan-komplexet istället för det stora zeolit-komplexet för att få fram mer information om hur inbindning av metalloxiden sker.

Det system jag undersökt har två olika ligandtyper för den ena metallkomplexet – β-diketonatligander och aminoalkohol-ligander – och två olika alkoxidgrupper (metoxid och etoxid) i det andra metallkomplexet i reaktionen. Synteserna gav väldefinierade komplex som användes i materialframställning. Tunnfilmerna var mycket jämna och nanopulverna var porösa. Toluen som lösningsmedel visade sig vara utmärkt med hög vätningsförmåga på de olika underlagen. Zeolit-komplexet kan användas som katalysator vid oxidation av metanol och silsesquioxan-komplexet kan användas som modell för zeoliter impregnerade med metalloxid.

References

1. Berzelius, J. J., *Edinburgh New Philos. J.*, **21** (1836) 223.
2. Schreyeck, L., A. Wlosik, and H. Fuzellier, *J. Mater. Chem.*, **11** (2001) 483-486.
3. West, A. R., *Basic Solid State Chemistry*, 2nd. ed, John Wiley & Sons, Chichester, 2001.
4. From: http://www.ifw-dresden.de/imw/. Accessed 2005-02-25.
5. From: http://www.veeco.com/learning/default.asp. Accessed 2005-02-25.
6. Mathur, S., M. Veith, T. Ruegamer, E. Hemmer, and H. Shen, *Chem. Mater.*, **16** (2004) 1304-1312.
7. Rocheleau, R. E., Z. Zhang, J. W. Gilje, and J. A. Meesemarktscheffel, *Chem. Mater.*, **6** (1994) 1615-1619.
8. Dislich, H., *Angew. Chem.*, **83** (1971) 428-435.
9. Pati, R. K. and P. Pramanik, *J. Am. Ceram. Soc.*, **83** (2000) 1822-1824.
10. Varnier, O., N. Hovnanian, A. Larbot, P. Bergez, L. Cot, and J. Charpin, *Mater. Res. Bull.*, **29** (1994) 479-488.
11. Veith, M., M. Haas, and V. Huch, *Chem. Mater.*, **17** (2005) 95-101.
12. Kessler, V. G., *The Synthesis and Solution Stability of Alkoxide Precursors* in *Handbook of Sol-Gel Science and Technology. Processing, Characterization and Applications. Volume I: Sol-Gel Processing*, Kozuka, H., (Ed.), Sakka, S. (Series Ed.). Kluwer Academic Publishers, Norwell, USA, 2004 (p. 3-40).
13. Kessler, V. G., *J. Sol-Gel Sci. Tech.*, **32** (2004) 11-14.
14. Turova, N. Y., E. P. Turevskaya, V. G. Kessler, and M. I. Yanovskaya, *The Chemistry of Metal Alkoxides*, Kluwer Academic Publishers, Amsterdam, 2002.
15. Kessler, V. G., *Chem. Commun.*, (2003) 1213-1222.
16. Kessler, V. G., A. N. Panov, N. Y. Turova, Z. A. Starikova, A. I. Yanovsky, F. M. Dolgushin, A. P. Pisarevsky, and Y. T. Struchkov, *J. Chem. Soc., Dalton Trans.*, (1998) 21-29.
17. Hubert-Pfalzgraf, L. G., V. G. Kessler, and J. Vaissermann, *Polyhedron*, **16** (1997) 4197-4203.
18. Westin, G., M. Moustiakimov, and M. Kritikos, *Inorg. Chem.*, **41** (2002) 3249-3258.
19. Meerwein, H. and T. Bersin, *Ann.*, **476** (1929) 113.
20. Bradley, D. C., R. C. Mehrotra, and P. D. Gaur, *Metal Alkoxides*, Academic Press, London, 1978.
21. Sanchez, C., R. Ribot, and S. Doeuff, *Transition Metal Oxo Polymers Synthesized via Sol-Gel Chemistry* in *Inorganic and Organometallic Polymers wuth Special Properties*, Laine, R. M., (Ed.). Kluwer Academic Publishers, The Netherlands, 1992 (p. 267-295).
22. Sirio, C., O. Poncelet, L. G. HubertPfalzgraf, J. C. Daran, and J. Vaissermann, *Polyhedron*, **11** (1992) 177-184.
23. Johansson, A. and V. G. Kessler, *Inorg. Chem. Comm.*, **3** (2000) 5-7.
24. Guillon, H., L. G. Hubert-Pfalzgraf, and J. Vaissermann, *Eur. J. Inorg. Chem.*, **6** (2000) 1243-1252.
25. Poncelet, O., L. G. HubertPfalzgraf, and J. C. Daran, *Inorg. Chem.*, **29** (1990) 2883-2885.
26. Pohl, A., *Sol-Gel Synthesis of CMR Manganites*, Doctoral Thesis, (2004) Uppsala University, Uppsala.
27. Westin, G., M. Wijk, and A. Pohl, *J. Sol-Gel Sci. Tech.*, **31** (2004) 283-286.
28. Turova, N. Y., A. I. Yanovskii, V. G. Kessler, N. I. Kozlova, and Y. T. Struchkov, *Russ. J. Inorg. Chem.*, **36** (1991) 1404-1407.
29. Moustiakimov, M., M. Kritikos, and G. Westin, *Acta Crystallogr., Sect. C: Cryst. Struct. Commun.*, **57** (2001) 515-516.
30. Moustiakimov, M., M. Kritikos, and G. Westin, *Inorg. Chem.*, **44** (2005) 1499-1504.
31. Kritikos, M., M. Moustiakimov, M. Wijk, and G. Westin, *J. Chem. Soc., Dalton Trans.*, (2001) 1931-1938.
32. Brinker, C. J. and G. W. Scherer, *Sol-Gel Science - The Physics and Chemistry of Sol-Gel Processing*, Academic Press, San Diego, 1990.

33. Ko, E. I., *Sol-Gel Process* in *Preparation of Solid Catalysts*, Ertl, G., H. Knözinger, and J. Weitkamp, (Eds.). Wiley-VCH, Weinhem, 1999 (p. 85-98).
34. Thomas, J. M., T. Maschmeyer, B. F. G. Johnson, and D. S. Shephard, *J. Mol. Catal. A*, **141** (1999) 139-144.
35. Sabater, M. J., A. Corma, A. Domenech, V. Fornés, and H. García, *Chem. Commun.*, **14** (1997) 1285-1286.
36. Ogunwumi, S. B. and T. Bein, *Chem. Commun.*, **9** (1997) 901-902.
37. Thomas, J. M., L. A. Bursill, and E. A. Lodge, *J. Chem. Soc., Chem. Comm.*, (1981) 276-277.
38. Schulz-Ekloff, G. and S. Ernst, *Zeolite-Entrapped Metal Complexes* in *Preparation of Solid Catalysts*, Ertl, G., H. Knözinger, and J. Weitkamp, (Eds.). Wiley-VCH, 1999 (p. 405-427).
39. SHELXTL 5.3 Reference Manual, Bruker AXS, Madison, WI, USA, 1997.
40. Jalilehvand, F., *Structure of Hydrated Ions and Cyano Complexes by X-Ray Absorption Spectroscopy*, Doctoral thesis, (2000) Kungliga Tekniska Högskolan, Stockholm.
41. George, G. N. and I. J. Pickering, EXAFSPAK - A Suite of Computer Programs for Analysis of X-Ray Absorption Spectra; George, G. N., Pickering, I. J. (Eds.), SSRL, Stanford, CA., 1993.
42. Zabinsky, S. I., J. J. Rehr, A. Ankudinov, R. C. Albers, and M. J. Eller, *Phys. Rev. B*, **52** (1995) 2995-3009.
43. Ankudinov, A., Ph. D. Thesis, (1996) University of Washington.
44. The FEFF program available from: http://Feff.phys.washington.edu/feff.
45. Huheey, J. E., E. A. Keiter, and R. L. Keiter, *Inorganic Chemistry: Principles of Structure and Reactivity*, 4th. ed, HarperCollins College Publishers, New York, 1993.
46. Shannon, R. D., *Acta Crystallogr., Sect. A: Fundam. Crystallogr.*, **32** (1976) 751-767.
47. Wright, D. A. and D. A. Williams, *Acta Crystallogr., Sect. B: Struct. Sci.*, **24** (1968) 1107-1114.
48. JCPDS Powder Diffraction Database, File card number, 1997, International Centre for Diffraction Data, Newtown Square, PA, USA.
49. Kessler, V. G., S. Gohil, M. Kritikos, O. N. Korsak, E. E. Knyazeva, I. F. Moskovskaya, and B. V. Romanovsky, *Polyhedron*, **20** (2001) 915-922.
50. Crocker, M., R. H. M. Herold, A. G. Orpen, and M. T. A. Overgaag, *J. Chem. Soc., Dalton Trans.*, (1999) 3791-3804.
51. Edelmann, F. T., S. Giessmann, and A. Fischer, *J. Organomet. Chem.*, **620** (2001) 80-89.
52. Edelmann, F. T., S. Giessmann, and A. Fischer, *Inorg. Chem. Comm.*, **3** (2000) 658-661.
53. Feher, F. J., D. A. Newman, and J. F. Walzer, *J. Am. Chem. Soc.*, **111** (1989) 1741-1748.
54. Feher, F. J., T. A. Budzichowski, R. L. Blanski, K. J. Weller, and J. W. Ziller, *Organometallics*, **10** (1991) 2626-2528.
55. Feher, F. J. and T. A. Budzichowski, *Polyhedron*, **14** (1995) 3239-3253.
56. Fei, Z. F., K. Ibrom, and F. T. Edelmann, *Z Anorg. Allg. Chem.*, **628** (2002) 2109-2112.
57. Fei, Z. F., R. Schmutzler, and F. T. Edelmann, *Z Anorg. Allg. Chem.*, **629** (2003) 353-356.
58. Fei, Z. F., S. Busse, and F. T. Edelmann, *J. Chem. Soc., Dalton Trans.*, (2002) 2587-2589.
59. Gun'ko, Y. K., R. Reilly, F. T. Edelmann, and H. G. Schmidt, *Angew. Chem. Int. Ed. Engl.*, **40** (2001) 1279-1281.
60. Lorenz, V., M. Spoida, A. Fischer, and F. T. Edelmann, *J. Organomet. Chem.*, **625** (2001) 1-6.
61. Lorenz, V., A. Fischer, and F. T. Edelmann, *J. Organomet. Chem.*, **647** (2002) 245-249.
62. Lorenz, V., A. Fischer, K. Jacob, and F. T. Edelmann, *Inorg. Chem. Comm.*, **6** (2003) 795-798.
63. Lorenz, V., A. Fischer, and F. T. Edelmann, *Z Anorg. Allg. Chem.*, **626** (2000) 1728-1730.

Acknowledgments

The **Stanford Synchrotron Radiation Laboratory** is greatly acknowledged for making it possible to perform measurements at beamline 4-1. Portions of this research were carried out at the Stanford Synchrotron Radiation Laboratory, a national user facility operated by Stanford University on behalf of the U.S. Department of Energy, Office of Basic Energy Sciences. The SSRL Structural Molecular Biology Program is supported by the Department of Energy, Office of Biological and Environmental Research, and by the National Institutes of Health, National Center for Research Resources, Biomedical Technology Program.